Threshold Dynamics for Anisotropic Surface Energies*

Matt Elsey† Courant Institute

Selim Esedoḡlu‡ University of Michigan

April 21, 2016

Abstract

We study extensions of Merriman, Bence, and Osher's threshold dynamics scheme to weighted mean curvature flow, which arises as gradient descent for anisotropic (normal dependent) surface energies. In particular, we investigate, in both two and three dimensions, those anisotropies for which the convolution kernel in the scheme can be chosen to be positive and / or to possess a positive Fourier transform. We provide a complete, geometric characterization of such anisotropies. This has implications for the unconditional stability and, in the two-phase setting, the monotonicity, of the scheme. We also revisit previous constructions of convolution kernels from a variational perspective, and propose a new one. The variational perspective differentiates between the normal dependent mobility and surface tension factors (both of which contribute to the normal speed) that results from a given convolution kernel. This more granular understanding is particularly useful in the multiphase setting, where junctions are present.

1 Introduction

Threshold dynamics – also known as diffusion or convolution generated motion – is a very efficient algorithm for approximating the motion by mean curvature of an interface. It was introduced by Merriman, Bence, and Osher (MBO) in [21, 20]. Motion by mean curvature arises as L^2 gradient descent for perimeter of sets. Perimeter of sets, in turn, often arises as a penalty term in variational models for interfaces in a great variety of applications, ranging from image processing and computer vision (e.g. the Mumford-Shah model [23] for image segmentation) to materials science (e.g. Mullins' model [22] for grain boundary motion in polycrystals). The MBO scheme, its variants, and its extensions have attracted sustained interest in the context of each one of these applications.

*Mathematics subject classification: 65M12 (primary), 35K93.

†Currently at Intel Corporation. Email: melsey@cims.nyu.edu

‡Corresponding author. Email: esedoglu@umich.edu

In this paper, we discuss the extension of the threshold dynamics to anisotropic (weighted) mean curvature motions, which arise as gradient descent for interfacial energies with normal dependent densities. This entails replacing the Gaussian kernel used in the convolution step of the original algorithm with more general kernels that are possibly not radially symmetric. There is already considerable literature on this problem; in particular, previous authors have tackled the question of how to construct a convolution kernel for a given anisotropy. A summary touching on the prior work most relevant for the discussion in this paper can be found below in Section 3.

Our main goal is to explore the positivity properties, in physical and Fourier domains, that can be demanded of the convolution kernels used in this context. Using a convolution kernel that is positive in the physical domain endows two-phase threshold dynamics with a comparison principle (monotonicity), and thus has immediate implications for its stability and convergence. Positivity of the convolution kernel in the Fourier domain, on the other hand, endows threshold dynamics with an energy dissipation property which, unlike the comparison principle, can be extended to certain multi-phase situations [8]. It is therefore also natural to investigate the type of anisotropies for which a convolution kernel can be constructed that is positive in both the physical and Fourier domains. We give a complete, geometric answer to these questions (which turn out to depend on dimension) in terms of the Wulff shape of the anisotropy. Our answer, stated in Theorem 11 and contained in Section 5.4, also provides a new approach to kernel construction that is, in an appropriate sense, maximally positive.

The variational (minimizing movements) interpretation of threshold dynamics given in [8] provides guidance in our discussion. We revisit some of the previous kernel constructions in the literature, especially [26], from this perspective, and identify separately the surface tension and mobility factors that correspond to the proposed kernel, both of which contribute to the normal speed of an interface evolved by the threshold dynamics algorithm. This more granular understanding promises to be particularly useful in extending anisotropic threshold dynamics to the multiphase setting of networks of surfaces, which we demonstrate with a numerical example in Section 6.

2 Preliminaries and Notation

Given a non-negative, continuous, even function $\sigma : \mathbb{S}^{d-1} \to \mathbb{R}^+$ with $\sigma(x) > 0$ for $x \neq 0$, we consider the two-phase, possibly anisotropic surface energy

$$E(\Sigma) = \int_{\partial\Sigma} \sigma(n(x))\, dS(x) \tag{1}$$

where Σ is a set in $\mathbb{R}^d$, dS denotes the surface measure on its boundary $\partial\Sigma$, and $n(x)$ denotes the outward unit normal to $\partial\Sigma$. We will also consider the

multi-phase extension of energy (1) to partitions:

$$E(\Sigma_1, \ldots, \Sigma_N) = \sum_{\substack{i,j=1 \\ i \neq j}}^{N} \int_{(\partial\Sigma_i)\cap(\partial\Sigma_j)} \sigma_{i,j}(n(x))\, dS \tag{2}$$

where $\Sigma_1, \ldots, \Sigma_N$ satisfy

$$\bigcup_{i=1}^{N} \Sigma_i = D \text{ and } \Sigma_i \cap \Sigma_j = (\partial\Sigma_i) \cap (\partial\Sigma_j) \text{ for } i \neq j \tag{3}$$

where D, the computational domain, is typically a cube in $\mathbb{R}^d$ with periodic boundary conditions, and $\sigma_{i,j}$ are subject to the same conditions as σ above. It will be convenient to assume that σ has been extended to $\sigma : \mathbb{R}^d \to \mathbb{R}^+$ as

$$\sigma(x) = |x|\sigma\left(\frac{x}{|x|}\right) \text{ for } x \neq 0$$

so that it is positively 1-homogeneous. Define the unit ball (i.e. the *Frank diagram)* B_σ *of* σ *as*

$$B_\sigma = \{x \,:\, \sigma(x) \leq 1\}$$

which is thus a closed, convex, centrally symmetric set. We require B_σ to be smooth and strictly convex; this condition will ensure well-posedness of the two-phase energy (1) and also imply that we stay clear of the crystalline cases (where B_σ is a polytope) except via approximation. In two dimensions, we will also write $\sigma = \sigma(\theta)$, where θ is the angle that the unit normal makes with the positive x_1-axis. In that case, strict convexity of B_σ is equivalent to the condition

$$\sigma''(\theta) + \sigma(\theta) > 0.$$

The *Wulff shape* W_σ associated with the anisotropy σ is defined as

$$W_\sigma = \left\{ y \,:\, \sup_{x \in B_\sigma} x \cdot y \leq 1 \right\}.$$

The sets B_σ can in turn be obtained from W_σ by the formula

$$B_\sigma = \left\{ x \,:\, \sup_{y \in W_\sigma} x \cdot y \leq 1 \right\},$$

exhibiting the well known duality between B_σ and W_σ .

For $x \in \mathbb{R}^d$, $x = (x_1, \ldots, x_d)$, write $x' = (x_1, \ldots, x_{d-1})$ so that $x = (x', x_d)$. Let $e_1, \ldots, e_d$ be the standard basis. We will denote the *Radon transform* of a function $f : \mathbb{R}^d \to \mathbb{R}$ by

$$\mathcal{J}f(n, r) = \int_{\{x \,:\, \langle x, n\rangle = r\}} f(x)\, dH^{d-1}(x) \tag{4}$$

where H^d denotes the d-dimensional Hausdorff measure. We will denote the *spherical Radon transform* of an even function $f : \mathbb{S}^{d-1} \to \mathbb{R}$ by

$$\mathcal{J}_s f(n) = \int_{\mathbb{S}^{d-1} \cap n^\perp} f(x)\, dH^{d-1}(x). \tag{5}$$

We will use the following definition of the Fourier transform on $\mathbb{R}^d$:

$$\widehat{f}(\xi) = \int_{\mathbb{R}^d} f(x) e^{-ix\cdot\xi}\, d\xi \text{ so that } f(x) = \frac{1}{(2\pi)^d} \int_{\mathbb{R}^d} \widehat{f}(\xi) e^{i\xi\cdot x}\, d\xi$$

for e.g. f in Schwartz class.

For $d = 2$ or 3, we will study approximations for L^2 gradient flow of energies (1) and (2), which are known as weighted mean curvature flow (of an interface and a network). The normal speed of an interface in three dimensions under this flow is given by

$$v_\perp(x) = \mu(n(x)) \left(\left(\partial_{s_1}^2 \sigma(n(x)) + \sigma(n(x)) \right) \kappa_1(x) + \left(\partial_{s_2}^2 \sigma(n(x)) + \sigma(n(x)) \right) \kappa_2 \right) \tag{6}$$

where κ_1 and κ_2 are the two principal curvatures, and ∂_{s_i} denotes differentiation along the great circle on $\mathbb{S}^2$ that passes through $n(x)$ and has as its tangent the i-th principal curvature direction. In the isotropic setting, the expression simplifies to

$$v_\perp(x) = \mu(n(x))\sigma(n(x)) \left(\kappa_1(x) + \kappa_2(x) \right). \tag{7}$$

In addition to (6), a condition known as the *Herring angle condition* [12] holds along triple junctions: For $d = 3$, at a junction formed by the meeting of the three phases Σ_i, Σ_j , and Σ_k , this condition reads

$$\begin{aligned}(\ell \times n_{i,j})\sigma_{i,j}(n_{i,j}) + (\ell \times n_{j,k})\sigma_{j,k}(n_{j,k}) + (\ell \times n_{k,i})\sigma_{k,i}(n_{k,i}) \\ + n_{j,i}\sigma'_{i,j}(n_{i,j}) + n_{k,j}\sigma'_{j,k}(n_{j,k}) + n_{i,k}\sigma'_{k,i}(n_{k,i}) = 0\end{aligned} \tag{8}$$

where $n_{i,j}$ is the unit normal vector to the interface $(\partial\Sigma_i) \cap (\partial\Sigma_j)$ pointing in the Σ_i to Σ_j direction, $\ell = n_{j,k} \times n_{i,j}$ is a unit vector tangent to the triple junction, and $\sigma'_{i,j}(n_{i,j})$ denotes derivative of $\sigma_{i,j}$ taken on $\mathbb{S}^2$ in the direction of the vector $\ell \times n_{i,j}$. In the isotropic setting, (8) simplifies to the following more familiar form, known as Young's law:

$$\sigma_{i,j} n_{i,j} + \sigma_{j,k} n_{j,k} + \sigma_{k,i} n_{k,i} = 0.$$

We note an important distinction between the two and three dimensional versions of (6). In two dimensions, (6) can be written as

$$v_\perp(x) = \mu(\theta(x)) \left(\sigma''(\theta(x)) + \sigma(\theta(x)) \right) \kappa(x) \tag{9}$$

where $\theta(x)$ is the angle that the outward unit normal $n(x)$ to $\partial\Sigma$ at x makes with the positive x_1-axis. If $\bar{\sigma}$ is another anisotropy in two dimensions, (9) can also be written as

$$v_\perp(x) = \bar{\mu}(\theta(x)) \left(\bar{\sigma}''(\theta(x)) + \bar{\sigma}(\theta(x)) \right) \kappa(x) \tag{10}$$

provided that we choose the new mobility $\bar{\mu}$ as

$$\bar{\mu}(\theta) = \mu(\theta)\frac{(\sigma''(\theta)+\sigma(\theta))}{(\bar{\sigma}''(\theta)+\bar{\sigma}(\theta))} > 0. \tag{11}$$

In words, weighted curvature flow in two dimensions with respect to an anisotropy σ can masquerade as flow for any other anisotropy via an appropriate choice of the mobility factor. In particular, all anisotropic flows of the form (9) decrease every surface energy of the form (1). This is no longer the case in three dimensions:

Proposition 1. *In three dimensions, the solution operator $\mathcal{S}_{\sigma,\mu}$ for the evolution (6) determines the two factors $\sigma, \mu : \mathbb{S}^2 \to \mathbb{R}^+$ uniquely up to a constant multiplicative factor.*

Proof. Start by observing that for $p \in \mathbb{S}^2$ and $v \in T_p$ with $|v| = 1$, we have

$$\langle (D^2\sigma)_p v, v\rangle = \sigma_{vv}(p) + \sigma(p)$$

where σ_{vv} denotes differentiation in the direction of the vector v *on the unit sphere* (whereas the left hand side derivatives are in $\mathbb{R}^3$ taken on the positively one-homogeneous extension of σ). Suppose that we have two distinct anisotropies σ^1 and σ^2 that lead to the same normal speed for all interfaces up to a mobility factor μ, i.e.

$$\sum_{j=1}^{2}\langle (D^2\sigma^1)_p v_j(p), v_j(p)\rangle \kappa_j(p) = v_\perp^1 = v_\perp^2 = \mu(p)\sum_{j=1}^{2}\langle (D^2\sigma^2)_p v_j(p), v_j(p)\rangle \kappa_j(p)$$

for all p and v on $\mathbb{S}^2$. First, we observe that by restricting attention to *cylinders* as interfaces on which to evaluate the equality above (so that one of the principal curvatures is 0), we obtain:

$$\langle (D^2\sigma^1)_p v, v\rangle = \mu(p)\langle (D^2\sigma^2)_p v, v\rangle \text{ for all } p, v \in \mathbb{S}^2 \text{ with } v \cdot p = 0.$$

The equality is obtained by observing that the cylinder can be spun at any point about its normal p at that point, whence the principal curvature direction corresponding to the non-zero principal curvature can be chosen to be any vector $v \perp p$. Noting further that $(D^2\sigma^j)_p p = 0$ for $j = 1$ and $j = 2$, we in fact have

$$\langle (D^2\sigma^1)_p v, v\rangle = \mu(p)\langle (D^2\sigma^2)_p v, v\rangle \text{ for all } p \in \mathbb{S}^2 \text{ and all } v.$$

Extend μ to a neighborhood of $\mathbb{S}^2$ in a zero-homogeneous manner (constant along radial directions). By the 1-homogeneity of σ^i , we have

$$\left(D^2\sigma^i\right)_p = \frac{1}{|p|}\left(D^2\sigma^i\right)_{\frac{p}{|p|}}.$$

Therefore, we have:

$$\left\langle \left(D^2\sigma^1\right)_p u, u\right\rangle = \mu(p)\left\langle \left(D^2\sigma^2\right)_p u, u\right\rangle$$

for all p near $\mathbb{S}^2$ and all $u \in \mathbb{R}^3$. Since the matrices are symmetric, that implies

$$\left(D^2\sigma^1\right)_p = \mu(p)\left(D^2\sigma^2\right)_p$$

for all p near $\mathbb{S}^2$. We now claim that μ is constant on $\mathbb{S}^2$. To see this, note that the rows of the matrix equation

$$\left(D^2\sigma^1\right)_p = \mu(p)\left(D^2\sigma^2\right)_p$$

read

$$\nabla\left(\partial_{x_i}\sigma^1\right) = \mu\nabla\left(\partial_{x_i}\sigma^2\right).$$

Taking the curl of both sides, we get:

$$\nabla \times \left(\mu\nabla\left(\partial_{x_i}\sigma^2\right)\right) = 0.$$

Using the identity

$$\nabla \times (gF) = g\nabla \times F + \nabla g \times F$$

we find

$$\nabla\mu \times \nabla\left(\partial_{x_i}\sigma^2\right) = 0.$$

By strict convexity of the Wulff shape corresponding to σ^2 , at every point $p \neq 0$ the matrix $\left(D^2\sigma^2\right)_p$ has two strictly positive eigenvalues the corresponding eigenvectors of which span T_p. Thus, the columns $\nabla\left(\partial_{x_i}\sigma^2\right)$ of $D^2\sigma^2$ span T_p. Since by 0-homogeneity of μ we already know that $\nabla\mu \perp p$, this implies $\nabla\mu = 0$. □

3 Previous work and kernels

In the simplest two-phase setting, Merriman, Bence, and Osher's threshold dynamics algorithm as presented in the original paper [20] has the following form:

Algorithm: (Merriman, Bence, Osher'92): Alternate the following steps:

1. Convolution:

$$\psi^k = \frac{1}{(\delta t)^{\frac{d}{2}}} K\left(\frac{x}{\sqrt{\delta t}}\right) * \mathbf{1}_{\Sigma^k} \tag{12}$$

2. Thresholding:

$$\Sigma^{k+1} = \left\{x \,:\, \psi^k(x) \geq \frac{1}{2}\right\}. \tag{13}$$

where the convolution kernel K satisfies

$$K(x) = K(-x) \text{ and } \int_{\mathbb{R}^d} K(x)\, dx = 1 \tag{14}$$

For convenience, we will write

$$K_{\delta t}(x) = \frac{1}{(\delta t)^{\frac{d}{2}}} K\left(\frac{x}{\sqrt{\delta t}}\right).$$

In the original papers [21, 20], the kernel K is taken to be the Gaussian:

$$G(x) = \frac{1}{(4\pi)^{\frac{d}{2}}} \exp\left(-\frac{|x|^2}{4}\right)$$

although the possibility of choosing it to be not necessarily radially symmetric for anisotropic curvature motions is also mentioned.

In addition to (14), we will make the following natural assumptions on the kernel K which are close to, but slightly different than, the ones in [15]. They confer sufficient decay and regularity on K to justify the elementary Taylor expansion entailed in the consistency calculation given in the Appendix which closely follows the one in [15]. Moreover, most of the explicit kernel constructions in the literature so far, e.g. in [26] and [6], satisfy these properties. They are:

1. There exists $C > 0$ and $p > d + 1$ such that

$$|K(x)| \leq \frac{C}{1 + |x|^p}. \tag{15}$$

2. We have

$$\lim_{\varepsilon \to 0} \sup_{\mathcal{O} \in \mathbf{O}} \int_{\mathbb{R}^{d-1}} |K \circ \mathcal{O}(x', \varepsilon g(x')) - K \circ \mathcal{O}(x', 0)| \left(1 + |x'|^2\right)\, dx' = 0 \tag{16}$$

   for every map $g : \mathbb{R}^{d-1} \to \mathbb{R}^{d-1}$ of the form

$$g(x') = \langle Mx', x' \rangle + a$$

   where M is a $(d-1) \times (d-1)$ symmetric matrix and $a \in \mathbb{R}$, and $\mathbf{O}$ is the set of $(d-1) \times (d-1)$ orthogonal matrices.

3. For every $(d-1) \times (d-1)$ orthogonal matrix $\mathcal{O}$,

$$\int_{\mathbb{R}^{d-1}} K \circ \mathcal{O}(x', 0)\, dx' > 0 \tag{17}$$

Note that choosing $M = 0$ and $a = 1$ in Assumption (16), we get

$$\lim_{r \to 0} \int_{\mathbb{R}^{d-1}} K \circ \mathcal{O}(x', r)\, dx' = \int_{\mathbb{R}^{d-1}} K \circ \mathcal{O}(x', 0)\, dx' \tag{18}$$

for every orthogonal matrix $\mathcal{O}$. Also note that for any $\gamma \in [0, 1 - \frac{1}{p-d})$ and $r > 0$, we have

$$\begin{aligned} \int_{|x|\geq r\varepsilon^{\gamma}} |K_{\varepsilon^2}(x)|\, dx &= \int_{|x|\geq r\varepsilon^{\gamma-1}} |K(x)|\, dx \\ &\leq \int_{|x|\geq r\varepsilon^{\gamma-1}} \frac{C}{1+|x|^p}\, dx \\ &\leq C\left(r\varepsilon^{1-\gamma}\right)^{p-d} = o(\varepsilon) \end{aligned} \tag{19}$$

as $\varepsilon \to 0$ by Assumption (15) on the kernel K.

With a radially symmetric kernel K satisfying Assumptions (14)-(17), Algorithm (12) & (13) can be seen to generate a discrete in time approximation to the isotropic motion by mean curvature of a smooth initial interface $\partial\Sigma^0$ by a simple Taylor expansion of the convolution in (12) in powers of $\sqrt{\delta t}$; this calculation was carried out, in the case of a Gaussian, first in [25, 19]. Positivity of the kernel K endows the scheme with a comparison principle: Both steps of the Algorithm (12) & (13) are seen in this case to be monotone. Accordingly, the comparison principle has been a key tool in studying convergence of the algorithm e.g. in [9, 4].

In [8], a variational formulation for the original MBO scheme (12) & (13) was given. In particular, it was shown that the following functional defined on sets, with kernel K chosen to be the Gaussian G, turns out to be a non-local approximation to (isotropic) perimeter, and is dissipated by the MBO scheme at every step, regardless of time step size:

$$E_{\delta t}(\Sigma) = \frac{1}{\sqrt{\delta t}} \int_{\Sigma^c} K_{\delta t} * \mathbf{1}_{\Sigma}\, dx. \tag{20}$$

Thus, (20) is a Lyapunov functional for algorithm (12) & (13), establishing its unconditional gradient stability. Moreover, the following *minimizing movements* [2, 18] interpretation involving (20) for algorithm (12) & (13) was given:

$$\Sigma^{k+1} = \arg\min_{\Sigma} E_{\delta t}(\Sigma) + \frac{1}{\sqrt{\delta t}} \int (\mathbf{1}_{\Sigma} - \mathbf{1}_{\Sigma^k}) K_{\delta t} * (\mathbf{1}_{\Sigma} - \mathbf{1}_{\Sigma^k})\, dx \tag{21}$$

where the kernel K was again taken to be G. In [8], variational formulation (20) & (21) was also extended to the *multiphase* setting.

Following the original threshold dynamics paper [21], there have been multiple contributions to the question of just what type of anisotropies are treatable by an algorithm of the form (12) & (13). All previous studies in this vein focus exclusively on the two-phase setting. One of the first contributions to this question is [15] by Ishii, Pires, and Souganidis. The core content of their paper is the derivation of the expression for the normal speed of an interface evolved by threshold dynamics using a given positive but possibly not radially symmetric convolution kernel (that, in addition, satisfies certain decay and regularity properties). Combined with the comparison principle that is immediate from

positivity assumption on the kernel, they are able to establish convergence of the two-phase algorithm to the viscosity solution of the corresponding geometric flow under the assumption that fattening of the viscosity solution does not occur. This result follows from essentially a Taylor expansion for the smooth interface after one step of the scheme to check consistency, and using the stability implied by the comparison principle that holds for the scheme as long as the convolution kernel is positive.

The reverse question of how to find the convolution kernel to be used in threshold dynamics for a given anisotropy is not addressed in the paper [15] of Ishii et. al. The first contribution in this direction we are aware of came in [26] by Ruuth and Merriman. There, the authors focus on the normal speed generated by the scheme in two dimensions, and construct a kernel of the form $\mathbf{1}_\Omega(x)$ where the centrally symmetric set $\Omega \subset \mathbb{R}^2$ is chosen so that scheme (12) & (13) is consistent with the normal speed

$$v_n = \big(f''(\theta) + f(\theta)\big)\kappa$$

where $f : [0, 2\pi] \to \mathbb{R}$ is a given periodic function satisfying $f''+f > 0$. Although the authors' construction indeed leads to the advertised normal speed (e.g. by results of [15]), there is no discussion in their paper that in two dimensions the same normal speed may result from an infinite number of anisotropic surface tension and mobility pairs. We will revisit this in Section 5.2.

A more recent contribution to the question of how to construct a convolution kernel for a given anisotropy is [6] by Bonnetier, Bretin, and Chambolle. Their kernels are explicit in the Fourier domain in terms of the anisotropy σ:

$$\widehat{K}_{\delta t}(\xi) = \exp\big(-(\delta t)\sigma^2(\xi)\big) \tag{22}$$

and are shown to generate motion by a normal speed of the form

$$v_\perp(x) = \sigma(n(x))\left((\partial^2_{s_1}\sigma + \sigma)\kappa_1 + (\partial^2_{s_2}\sigma + \sigma)\kappa_2\right)$$

In particular, the mobility is the natural mobility – the one that leads to the evolution of the corresponding Wulff shape of the anisotropy in a stable, self-similar manner. These kernels are positive in the Fourier domain by construction – a fact that has important implications for the energetic formulation of convolution generated motion discussed in this paper, as explained in Section 4. However, as pointed out by the authors, they may not be positive in physical space, even for smooth, strictly convex approximations to an anisotropy as simple as $\sigma(x_1, x_2) = |x_1| + |x_2|$. Consequently, the comparison principle that holds for two-phase motion by normal speed (6) is not always maintained by convolution generated motion using these kernels. In Section 5.4, we will explore if it is possible to do better, i.e. whether, for a given anisotropy, perhaps a different construction might yield a kernel that is positive in physical space. The answer depends on the spatial dimension d.

4 Anisotropic energy and mobility of a kernel

In this section, we will discuss the variational interpretation of threshold dynamics contained in (20) and (21) in the context of anisotropic convolution kernels. Let us write the Lyapunov function (20) as

$$E_{K,\delta t}(\Sigma) = \frac{1}{\sqrt{\delta t}} \int_{\Sigma^c} K_{\delta t} * \mathbf{1}_\Sigma \, dx \tag{23}$$

to emphasize dependence on the kernel K, which we will assume to satisfy the conditions (14), (15), (16), and (17). As in [8], consider the following relaxed version of this energy

$$E_{K,\delta t}(u, v) = \frac{1}{\sqrt{\delta t}} \int v K_{\delta t} * u \, dx \tag{24}$$

where u and v are subject to the constraints

$$u, v \geq 0 \text{ and } u + v = 1. \tag{25}$$

Let us recall the following fact from [8] that ensures (23) is a Lyapunov functional for scheme (12) & (13), establishing the connection between the variational problem (23) and threshold dynamics, and underlining the significance of $\widehat{K}$:

Proposition 2. *([8]) If $\widehat{K} \geq 0$, threshold dynamics algorithm (12) & (13) decreases energy (23) at every time step, regardless of the time step size.*

Proof. Write the relaxed version (24) of energy (20), subject to constraint (25), as

$$E_{K,\delta t}(u) = \frac{1}{\sqrt{\delta t}} \int (1 - u) K_{\delta t} * u \, dx$$

where we eliminated the variable v using the second constraint in (25). We have:

$$E_{K,\delta t}(u) = \frac{1}{\sqrt{\delta t}} \int K_{\delta t}^{\frac{1}{2}} * (1 - u) \, K_{\delta t}^{\frac{1}{2}} * u \, dx$$

where $\widehat{K_{\delta t}^{\frac{1}{2}}} = \sqrt{\widehat{K_{\delta t}}}$. We see that $E_{K,\delta t}$ is a concave function of $K_{\delta t}^{\frac{1}{2}} * u$, which is a linear function of u. Thus, $E_{K,\delta t}$ is a concave function of u. Conclusion follows by observing that algorithm (12) & (13) can be realized as minimizing the linearization of $E_{K,\delta t}$ at the current configuration over the entire constraint set at every time step. □

Although [15] obtains an expression for the normal speed of an interface evolved by algorithm (12) & (13) in terms of the convolution kernel K, there do not appear to be explicit formulas for the *surface tension* and *mobility* factors associated with a general kernel K in the previous literature on anisotropic threshold dynamics (for non-local energies of type (20), [1] contains an expression for the corresponding surface tension in the form of a variational problem). The surface tension and mobility factors associated with the thresholding scheme

(12) & (13) for a general, possibly anisotropic kernel K can be easily motivated via the variational formulation in [8] simply by evaluating the energy (20) and movement limiter (21) on sets with smooth boundaries. In the following, we first note the limit as $\delta t \to 0$ of energies $E_{K,\delta t}$ on smooth interfaces, and obtain a simple expression for the corresponding surface tension:

Proposition 3. *Let Σ be a compact subset of $\mathbb{R}^d$ with smooth boundary. Let $K : \mathbb{R}^d \to \mathbb{R}$ be a kernel satisfying (14) and (15). Then:*

$$\lim_{\delta t \to 0^+} E_{K,\delta t}(\Sigma) = \int_{\partial\Sigma} \sigma_K\big(n(x)\big)\, dH^{d-1}(x)$$

where the surface tension $\sigma_K : \mathbb{R}^d \to \mathbb{R}^+$ is defined as

$$\sigma_K(n) := \frac{1}{2}\int_{\mathbb{R}^d} |n \cdot x| K(x)\, dx. \tag{26}$$

Proof. We recall from the consistency step of the gamma convergence statement in [8]:

$$\lim_{\delta t \to 0^+} \frac{1}{\sqrt{\delta t}} \int \mathbf{1}_{\boldsymbol{\Sigma}}(x - \sqrt{\delta t} y)\mathbf{1}_{\Sigma^c}(x)\, dx = \int_{\partial\Sigma} (n(x)\cdot y)_+ \, dH^{d-1}(x)$$

and

$$\begin{aligned} E_{K,\delta t}(\Sigma) &= \frac{1}{\sqrt{\delta t}} \int K_{\delta t}(y) \int \mathbf{1}_{\Sigma}(x-y)\mathbf{1}_{\Sigma^c}(x)\, dx\, dy \\ &= \int K(y) \frac{1}{\sqrt{\delta t}} \int \mathbf{1}_{\Sigma}(x - \sqrt{\delta t} y)\mathbf{1}_{\Sigma^c}(x)\, dx\, dy. \end{aligned}$$

Since

$$\frac{1}{\sqrt{\delta t}} \int \mathbf{1}_{\Sigma}(x - \sqrt{\delta t} y)\mathbf{1}_{\Sigma^c}(x)\, dx \le 2\,|y|\,\mathrm{Per}(\Sigma)$$

for all small enough δt , and $|y|\,K(y) \in L^1(\mathbb{R}^d)$ by assumption (15) on K, we get

$$\lim_{\delta t \to 0^+} E_{K,\delta t}(\Sigma) = \frac{1}{2}\int_{\mathbb{R}^d} K(y) \int_{\partial\Sigma} |n(x)\cdot y| \, dH^{d-1}(x)\, dy$$

by dominated convergence and symmetry (14) of K.

□

Let us record formula (26) in polar coordinates:

$$\sigma_K(n) = \frac{1}{2}\int_0^\infty r^d \int_{\mathbb{S}^{d-1}} |n\cdot x| K(rx)\, dH^{d-1}(x)\, dr. \tag{27}$$

Next, we obtain a formula for the mobility μ_K that corresponds to a given kernel K by evaluating the movement limiter term from (21), namely

$$\frac{1}{\sqrt{\delta t}} \int (\mathbf{1}_{\Sigma} - \mathbf{1}_{\Sigma^k}) \left[K_{\delta t} * (\mathbf{1}_{\Sigma} - \mathbf{1}_{\Sigma^k})\right] dx, \tag{28}$$

where Σ^k denotes the current configuration and Σ its perturbed version, again on a smooth interface, perturbed by a smooth vector field.

Proposition 4. *Let $\Sigma(0)$ be a compact set with C^2 boundary. Let the kernel K be continuous and satisfy (14) and (15). Let $\Sigma(t)$ denote $\Sigma(0)$ evolved under motion with normal speed*

$$v_\perp(x,t) = \phi(x)$$

where $\phi : \mathbb{R}^d \to \mathbb{R}$ is a smooth function. Then

$$\lim_{\delta t \to 0^+} \lim_{t \to 0^+} \frac{\sqrt{\delta t}}{t^2} \int \left(\mathbf{1}_{\Sigma(t)} - \mathbf{1}_{\Sigma(0)}\right) \left[K_{\delta t} * \left(\mathbf{1}_{\Sigma(t)} - \mathbf{1}_{\Sigma(0)}\right)\right] dx \\ = \int_{\partial\Sigma(0)} \frac{1}{\mu_K(n(x))} \phi^2(x)\, dH^{d-1}(x)$$

where the function $\mu_K : \mathbb{S}^{d-1} \to \mathbb{R}$ is given by

$$\mu_K(n) = \frac{1}{\mathcal{J}K(n,0)}. \tag{29}$$

Proof. We have

$$\lim_{t \to 0} \int K_{\delta t}(x-y) \left(\frac{\mathbf{1}_{\Sigma(t)}(y) - \mathbf{1}_{\Sigma(0)}(y)}{t}\right) dy = \int_{\partial\Sigma} K_{\delta t}(x-y)\phi(y)\, dH^{d-1}(y)$$

uniformly on bounded sets, by the standard calculation of first variation for $\int_{\Sigma(t)} K_{\delta t}(x-y)\, dy$. Then,

$$\lim_{t \to 0} \int \left(\frac{\mathbf{1}_{\Sigma(t)} - \mathbf{1}_{\Sigma(0)}}{t}\right) \left[K_{\delta t} * \left(\frac{\mathbf{1}_{\Sigma(t)} - \mathbf{1}_{\Sigma(0)}}{t}\right)\right] dx \\ = \int_{\partial\Sigma} \int_{\partial\Sigma} K_{\delta t}(x-y)\phi(x)\phi(y)\, dH^{d-1}(y)\, dH^{d-1}(x)$$

by the same token. That means

$$\int \left(\mathbf{1}_{\Sigma^c(t)} - \mathbf{1}_{\Sigma^c(0)}\right) \left[K_{\delta t} * \left(\mathbf{1}_{\Sigma(t)} - \mathbf{1}_{\Sigma(0)}\right)\right] dx \\ = t^2 \left\{ \int_{\partial\Sigma} \int_{\partial\Sigma} K_{\delta t}(x-y)\phi(x)\phi(y)\, dH^{d-1}(y)\, dH^{d-1}(x) + r_1(\delta t, t) \right\}$$

where, for each $\delta t > 0$, $r_1(\delta t, t) \to 0$ as $t \to 0$. Noting that for $x \in \partial\Sigma$

$$\sqrt{\delta t} \int_{\partial\Sigma} K_{\delta t}(x-y)\phi(y)\, dH^{d-1}(y) = \phi(x) \int_{y \cdot n(x) = 0} K(y)\, dH^{d-1}(y) + r_2(\delta t)$$

where $r_2(\delta t) \to 0$ as $\delta t \to 0$ due to (15) and the continuity of K, we reach the conclusion of the proposition. □

Remark 5. Proposition 29 can be established also for (possibly discontinuous) kernels K satisfying assumptions (14)-(17) by a calculation similar to that of Proposition 13 in the Appendix.

Although Propositions 3 and 4 provide valuable motivation, they do not establish a rigorous connection with their advertised surface tension and mobility formulas and the dynamics generated by algorithm (12) & (13). There are numerous missing steps to a full justification (see [17] for a rigorous convergence result for the dynamics in the isotropic case utilizing the variational formulation of threshold dynamics). For example, to ensure that threshold dynamics dissipates energy (20) – or, equivalently, for the movement limiter (28) to have its minimum at the current configuration and thereby act to *limit* motion – the Fourier transform $\widehat{K}$ of the kernel K needs to be positive, as discussed in Proposition 2. Even then, the gamma limit of energies (20) has been established only in the case K is positive.

However, we can verify directly that the normal speed of the interface under a general kernel K obtained in Proposition 13 is consistent with the claimed surface tension (26) and mobility (4):

Proposition 6. *One step of scheme (12) & (13) moves a smooth interface with the normal speed:*

$$v_\perp(x) = \mu_K(n(x))\Big(\big(\partial_{s_1}^2\sigma_K(n(x)) + \sigma_K(n(x))\big)\,\kappa_1(x) + \big(\partial_{s_2}^2\sigma_K(n(x)) + \sigma_K(n(x))\big)\,\kappa_2(x)\Big) \quad (30)$$

to leading order in δt, where σ_K and μ_K are given by (26) and (29) respectively.

Proof. Let $x \in \partial\Sigma$. Let $n(x)$ be the outward unit normal to $\partial\Sigma$ at x. Let v_1 and v_2 be the principal curvature directions at x, and let κ_1 and κ_2 be the corresponding principal curvatures. Define

$$\sigma_{K,\varepsilon}(x) = \int_{\mathbb{R}^d} \sqrt{(x\cdot y)^2 + \varepsilon}K(y)\,dy.$$

We have

$$\partial_{x_i}\sigma_{K,\varepsilon}(x) = \int_{\mathbb{R}^d} \frac{(x\cdot y)y_i}{\sqrt{(x\cdot y)^2+\varepsilon}}K(y)\,dy$$

and

$$\partial_{x_ix_j}\sigma_{K,\varepsilon}(x) = \int_{\mathbb{R}^d} \frac{\varepsilon y_iy_j}{((x\cdot y)^2+\varepsilon)^{\frac{3}{2}}}K(y)\,dy.$$

Using (16), it follows easily that in a neighborhood of any $x \neq 0$,

$$\partial_{x_i}\sigma_{K,\varepsilon}(x) \to \int_{y\cdot x=0} y_i(x\cdot y)K(y)\,dH^{d-1}(y)$$

uniformly, and

$$\partial_{x_ix_j}\sigma_{K,\varepsilon}(x) \to \int_{y\cdot x=0} y_iy_jK(y)\,dH^{d-1}(y)$$

uniformly. Thus, σ_K is C^2 near any $x \neq 0$, and

$$D^2\sigma_K(x) = \int_{y\cdot x=0} y \otimes y\, K(y)\, dy.$$

Therefore,

$$\begin{aligned}\left(\partial_{s_1}^2\sigma_K + \sigma_K\right)\kappa_1 + \left(\partial_{s_2}^2\sigma_K + \sigma_K\right)\kappa_2 &= \left\langle \left(D^2\sigma_K\right) v_1, v_1\right\rangle \kappa_1 + \left\langle \left(D^2\sigma_K\right) v_2, v_2\right\rangle \kappa_2 \\ &= \kappa_1 \int_{y\cdot n(x)=0} (v_1\cdot y)^2 K(y)\, dH^{d-1}(y) \\ &\quad + \kappa_2 \int_{y\cdot n(x)=0} (v_2\cdot y)^2 K(y)\, dH^{d-1}(y).\end{aligned} \tag{31}$$

The desired conclusion follows from (31) and Proposition 13. □

Since certain kernel constructions appearing in the literature, e.g. the construction of [6], are explicit in the Fourier domain, it is useful to express formulas (26) & (29) for the surface tension σ_K and mobility μ_K that correspond to a given convolution kernel K in terms of the Fourier transform $\widehat{K}$ of the kernel. We do this in the following proposition:

Proposition 7. *Let K satisfy (14) & (15). Assume that $\widehat{K}(n\xi)$, as a function of ξ, is Schwartz class for every $n \neq 0$. Then*

$$\begin{aligned}\sigma_K(n) &= -\frac{1}{\pi}\ F.\ P. \int_{\mathbb{R}} \frac{\widehat{K}(n\xi)}{\xi^2}\, d\xi \\ &= -\frac{1}{2\pi}\int_{\mathbb{R}} \frac{\widehat{K}(n\xi) - \widehat{K}(0)}{\xi^2}\, d\xi, \text{ and} \\ \mu_K(n) &= \frac{2\pi}{\int_{\mathbb{R}} \widehat{K}(n\xi)\, d\xi}.\end{aligned}$$

Proof. For $k = 1, 2, 3, \ldots$, let $\frac{1}{\xi^k}$ denote the tempered distribution $\phi \to$ F. P. $\int \frac{\phi(\xi)}{\xi^k}\, d\xi$ where ϕ is any Schwartz function. Recall that for the Heaviside function $H(x)$, we have

$$\widehat{H}(\xi) = \pi\delta(\xi) - \frac{i}{\xi}.$$

Since $|x| = xH(x) - xH(-x)$, we get

$$\widehat{|x|}(\xi) = i\left(\widehat{H}'(\xi) + \widehat{H}'(-\xi)\right) = -\frac{2}{\xi^2}.$$

Thus, for even ϕ, we have

$$\begin{aligned}\int_{\mathbb{R}} |x|\,\phi(x)\,dx &= \frac{1}{2\pi}\int \widehat{|x|}\widehat{\phi} \\ &= -\frac{1}{\pi}\ \text{F. P.}\int_{\mathbb{R}} \frac{\widehat{\phi}(\xi)}{\xi^2}\,d\xi \\ &= -2\frac{1}{\pi}\int_{\mathbb{R}} \frac{\widehat{\phi}(\xi)-\widehat{\phi}(0)}{\xi^2}\,d\xi\end{aligned} \tag{32}$$

where we used $\phi'(0) = 0$. Starting with the mobility μ_K, we have

$$\begin{aligned}\mu_K(n) &= \frac{1}{\mathcal{J}K(n,0)} \\ &= \frac{2\pi}{\int_{\mathbb{R}} \widehat{\mathcal{J}K}(n,\xi)e^{ir\xi}\,d\xi|_{r=0}} \\ &= \frac{2\pi}{\int_{\mathbb{R}} \widehat{K}(n\xi)\,d\xi}\end{aligned} \tag{33}$$

where we used the Fourier slice theorem $\widehat{\mathcal{J}K}(n,\xi) = \widehat{K}(n\xi)$, along with the hypothesis on $\widehat{K}$. Turning to the surface tension σ_K , we have

$$\begin{aligned}\sigma_K(n) &= \frac{1}{2}\int_{\mathbb{R}^d} |n\cdot x|\,K(x)\,dx \\ &= \frac{1}{2}\int_{\mathbb{R}} |r| \int_{x\cdot n=r} K(x)\,dH^{d-1}(x)\,dr \\ &= \frac{1}{2}\int_{\mathbb{R}} |r|\,\mathcal{J}K(n,r)\,dr \\ &= \frac{1}{4\pi}\int \widehat{|r|}\widehat{\mathcal{J}K}(n,\xi) \\ &= \frac{1}{4\pi}\int \widehat{|r|}\widehat{K}(r\xi) \\ &= -\frac{1}{2\pi}\ \text{F. P.}\int_{\mathbb{R}} \frac{\widehat{K}(r\xi)}{\xi^2}\,d\xi\end{aligned} \tag{34}$$

where we used the slice theorem again, as well as (32). □

5 Kernel construction

In this section, we will comment on the kernels constructed for the given anisotropies in several previous studies from the point of view of the energetic interpretation discussed above. We will also present a new construction. In our construction, we will emphasize the role of surface tensions over that of mobilities. There are multiple reasons for this. First, from the point of view of algorithm development, getting the correct behavior (8) at junctions in the multiphase setting

(2) turns out to be the hardest step. Mobilities, on the other hand, turn out to be relatively easy to obtain by slight modifications of the basic thresholding algorithm that do not alter its efficiency and simplicity, see e.g. [8]. Second, in materials science applications, such as grain boundary motion in polycrystals, it turns out that some of the most important statistical features of the evolution (e.g. grain size distribution, grain boundary character distribution [16]) do not appear to depend appreciably on the mobilities [14, 13]. Finally, in applications such as computer vision, the precise dynamics is less important than dissipating the right energy.

5.1 The cosine transform and zonoids

Before we begin, we introduce and discuss basic facts about an integral transform known as the *cosine transform* that will be important subsequently. In this section, we follow [10] and [5] for this and related transforms, and their geometric significance. These references also contain the correct history of and detailed attribution for the results we simply quote here.

Define the *cosine transform* Tf of an even function $f : \mathbb{S}^{d-1} \to \mathbb{R}$ as

$$Tf(n) = \int_{\mathbb{S}^{d-1}} f(n)|n \cdot x| \, dS(x). \tag{35}$$

It is thus a mapping of even functions on $\mathbb{S}^{d-1}$ back to even functions on $\mathbb{S}^{d-1}$. For $d = 2$, this can be written as

$$Tf(\theta) = \int_0^{2\pi} f(\bar{\theta})|\cos(\theta - \bar{\theta})| \, d\bar{\theta}. \tag{36}$$

We will need to be able to invert these transforms. We start with $d = 2$. In this case, (36) is a convolution, and therefore can be solved by the Fourier series. Indeed, f being even, we have

$$\widehat{f}(m) = e^{-im\pi}\widehat{f}(m)$$

and therefore

$$\widehat{f}(m) = 0 \text{ if } m \text{ is odd.}$$

Note that

$$\widehat{|\cos\theta|}(m) = \frac{4}{1-m^2}\cos\left(m\frac{\pi}{2}\right)\begin{cases} \frac{4}{1-m^2} & \text{if } m = 0 \pmod 4, \\ \frac{4}{m^2-1} & \text{if } m = 2 \pmod 4, \\ 0 & \text{otherwise} \end{cases}$$

so that

$$\frac{4}{1-m^2}\cos\left(m\frac{\pi}{2}\right)\widehat{w}(m) = \widehat{f}(m)$$

which means

$$f(\theta) = \frac{1}{4}\left(\partial_\theta^2 + I\right)Tf\left(\theta + \frac{\pi}{2}\right). \tag{37}$$

From this inversion formula, we see that

$$f(\theta) \geq 0 \text{ for all } \theta \text{ iff } (\mathrm{T}f)''(\theta) + Tf(\theta) \geq 0 \text{ for all } \theta. \tag{38}$$

This will be significant for us in terms of positivity of the convolution kernels we construct.

Inversion of (35) for $d = 3$ turns out to be more involved. A formula can be given by exploiting the following relationship between the cosine transform T and the *spherical Radon transform* $\mathcal{J}_s$:

$$(\Delta_{\mathbb{S}^2} + 2Id)\, T = \mathcal{J}_s$$

where $\Delta_{\mathbb{S}^2}$ is the surface Laplacian (the Laplace-Beltrami operator) on $\mathbb{S}^2$. Note that all three operators are symmetric, and commute with one another. Thus

$$T^{-1} = \mathcal{J}_s^{-1}\,(\Delta_{\mathbb{S}^2} + 2Id) = (\Delta_{\mathbb{S}^2} + 2Id)\,\mathcal{J}_s^{-1}. \tag{39}$$

There are classic inversion formulas available for the spherical Radon transform, see e.g. [11]. Of particular interest to us is a condition on Tf analogous to (38) that would ensure the positivity of f. In this regard, we also discuss an important class of convex bodies intimately connected with the cosine transform T.

A *zonotope* is defined to be a vector sum of line segments. As such, it is a convex, centrally symmetric polytope the support function of which can be written in the form

$$x \to \sum_{i=1}^{N} m_i |\langle x, v_i \rangle|$$

where $v_i \in \mathbb{S}^{d-1}$ and $m_i > 0$. A *zonoid* is a convex, centrally symmetric set that can be approximated by zonotopes with respect to the Hausdorff distance: the set of zonoids is defined to be the closure of the set of zonotopes in this metric. There are various characterizations of zonotopes. One of the most intuitive such says that a convex polytope with nonempty interior is a zonotope iff every $d-1$ dimensional face of it is a zonotope (and hence centrally symmetric). For instance, in two dimensions, every centrally symmetric convex polygon is a zonotope. In three dimensions, a cube is a zonotope (since its faces can be recognized as centrally symmetric polytopes), but an octahedron is not (triangles are not centrally symmetric). As limits of such special polytopes, zonoids turn out to be quite rare in high dimensions: Indeed, the set of zonoids is nowhere dense in the set of convex bodies for $d \geq 3$. Moreover, It turns out that a polytope is a zonoid if and only if it is already a zonotope. Therefore, an octahedron is in fact not even a zonoid. Thus, there is a neighborhood of the octahedron, in the Hausdorff metric, that contains no zonoids. The following is an important standard fact from the convex geometry literature that states an analogue of (38) in all dimensions:

Theorem 8. *([5],[10]) Given an even, smooth function $f : \mathbb{S}^{d-1} \to \mathbb{R}$, the following integral equation can be solved uniquely for the weight ω (called the generating distribution of f) among even, smooth functions on $\mathbb{S}^{d-1}$:*

$$f(n) = T\omega(n) = \int_{\mathbb{S}^{d-1}} \omega(n)|n \cdot x| \, dS(x).$$

The solution operator T^{-1} can be extended to all support functions of centrally symmetric convex bodies, taking its values among distributions on $\mathbb{S}^{d-1}$. Then, the distribution ω is a measure if and only if f is the support function of a zonoid.

5.2 Ruuth & Merriman kernels

In [26], Ruuth & Merriman consider, in two space dimensions, kernels of the following form

$$K(x) = \mathbf{1}_\Omega(x) \tag{40}$$

where $\Omega \subset \mathbb{R}^2$ is a compact, centrally symmetric set that is star shaped with respect to the origin. For any given positive, 2π-periodic, smooth function $f : \mathbb{R} \to \mathbb{R}$ that satisfies $f''(\theta) + f(\theta) > 0$ for all $\theta \in [0, 2\pi]$, the authors are able to choose the set Ω so that one step of threshold dynamics algorithm (12) & (13) moves the interface with normal speed

$$v_\perp = (f'' + f)\, \kappa. \tag{41}$$

Their approach is as follows: Describing the set Ω in polar coordinates

$$\Omega = \{(r\cos\theta, r\sin\theta) \, : \, 0 \le \theta \le 2\pi \text{ and } 0 \le r \le R(\theta)\}$$

where $R : [0.2\pi] \to \mathbb{R}$ is a continuous, periodic, positive function, the following Taylor expansion for the convolution step (13) of the threshold dynamics algorithm is obtained:

$$(\mathbf{1}_\Sigma * \mathbf{1}_\Omega)\left(p + y n_\Sigma(p)\right) \approx \frac{1}{2}|\Omega| - \frac{1}{3}\kappa(p)R^3\left(n_\Sigma^\perp(p)\right) - 2R\left(n_\Sigma^\perp(p)\right) y$$

where $p \in \partial\Sigma$ and $n_\Sigma(p)$ denotes the outward unit normal to $\partial\Sigma$ at p. The normal speed of the interface can be inferred from this, yielding

$$v_\perp(p) = \frac{1}{6}R^2\left(\theta + \frac{\pi}{2}\right)\kappa(p) \tag{42}$$

Based on (41) & (42), the authors conclude

$$f''(\theta) + f(\theta) = R^2\left(\theta + \frac{\pi}{2}\right) \tag{43}$$

which allows them to solve for $R(\theta)$ in terms of the given surface tension σ:

$$R(\theta) = \sqrt{f''\left(\theta - \frac{\pi}{2}\right) + f\left(\theta - \frac{\pi}{2}\right)}. \tag{44}$$

(44) in turn determines the set Ω so that the convolution kernel (40) generates motion by normal speed (41), as desired. The discussion in [26] does not explicitly identify a mobility or a surface tension corresponding to the authors' construction, however. In light of the ambiguity (9), (10) & (11) described in Section 2, normal speed (41) is in fact consistent with *any* anisotropy.

We now look at Ruuth & Merriman's construction (40) from the point of view of our discussion in Section 4. Formula (27) applied to (40) gives

$$\begin{aligned}\sigma_\Omega(\theta) &= \frac{1}{2}\int_0^\infty r^2 \int_0^{2\pi} |\cos(\theta-\theta')|\, \mathbf{1}_{[-R(\theta'),R(\theta')]}(r)\, d\theta'\, dr \\ &= \frac{1}{3}\int_0^{2\pi} R^3(\theta')\, |\cos(\theta-\theta')|\, d\theta'. \end{aligned} \tag{45}$$

But then, inversion formula (37) implies

$$R(\theta) = \sqrt[3]{\sigma''\left(\theta-\frac{\pi}{2}\right)+\sigma\left(\theta-\frac{\pi}{2}\right)} \tag{46}$$

up to a multiplicative constant. The upshot is that f appearing in (41) is *not* the correct surface tension associated with the Ruuth & Merriman construction, despite tempting appearances. The discrepancy can be explained by computing the mobility that corresponds to (40), using (29):

$$\mu(\theta) = \left(\int_{\partial H_\theta} \mathbf{1}_\Omega(y)\, dS(y)\right)^{-1} = \frac{1}{R\left(\theta+\frac{\pi}{2}\right)}. \tag{47}$$

Indeed, putting (46) & (47) together shows that both calculations give the same normal speed (42). Formulas (27) & (29) elucidate the contributions to this normal speed coming from the surface tension and the mobility factors, and show that a *different* surface tension (46) than the naive one (43) results from the choice of the kernel. The distinction would be significant, for example, in the multiphase setting, where surface tensions determine the angle conditions at junctions according to (8). This point is demonstrated in Section 6 with a numerical example featuring a triple junction.

5.3 Bonnetier, Bretin & Chambolle kernels

Since the kernels (22) in [6] cover the case of three dimensions, we know from Proposition 1 that there can be no ambiguity in their advertised mobility and surface tensions, unlike in Section 5.2. We can verify the resulting surface tension and mobility from these kernels easily using (26) & (29). For the surface

tension, we have:

$$\begin{aligned}\sigma_K(n) &= -\frac{1}{2\pi}\int_{\mathbb{R}} \frac{\widehat{K}(n\xi)-\widehat{K}(0)}{\xi^2}\,d\xi = -\frac{1}{2\pi}\int_{\mathbb{R}} \frac{\exp\left(-\sigma^2(n\xi)\right)-1}{\xi^2}\,d\xi \\ &= -\frac{1}{2\pi}\int_{\mathbb{R}} \frac{\exp\left(-\sigma^2(n)\xi^2\right)-1}{\xi^2}\,d\xi = -\frac{\sigma(n)}{2\pi}\int_{\mathbb{R}} \frac{e^{-x^2}-1}{x^2}\,dx \\ &= \frac{1}{\sqrt{\pi}}\sigma(n).\end{aligned}$$

The mobility is:

$$\begin{aligned}\mu_K(n) &= \frac{2\pi}{\int_{\mathbb{R}} \widehat{K}(n\xi)\,d\xi} = \frac{2\pi}{\int_{\mathbb{R}} \exp\left(-\sigma^2(n)\xi^2\right)\,d\xi} \\ &= \frac{2\pi\sigma(n)}{\int_{\mathbb{R}} \exp\left(-x^2\right)\,dx} = 2\sqrt{\pi}\sigma(n).\end{aligned}$$

These match the normal speed calculation in [6].

5.4 New kernels

The kernels constructed by Ruuth & Merriman are positive, but are restricted to two dimensions, and their Fourier transforms are not positive. The kernels constructed by Bonnetier et. al. are positive in the Fourier domain, but may not be positive in the physical domain, even for certain anisotropies in two dimensions, e.g. $\sigma(x_1, x_2) = |x_1| + |x_2|$. In this section, we will investigate the types of anisotropies, in two and three dimensions, for which we can expect to find convolution kernels that are positive in the physical domain, and perhaps simultaneously positive in the Fourier domain. Our first result in this direction is the following barrier theorem.

Theorem 9. *In three dimensions, a threshold dynamics algorithm (12) & (13) that is consistent with a weighted mean curvature motion (6) for some choice of the mobility $\mu : \mathbb{S}^2 \to \mathbb{R}^+$ and a surface tension $\sigma : \mathbb{S}^2 \to \mathbb{R}^+$ cannot possibly be monotone unless the Wulff shape W_σ corresponding to the surface tension σ is a **zonoid**. Moreover, if the Wulff shape of the anisotropy is not a zonoid, then a positive convolution kernel cannot be found for any other anisotropy the Wulff shape of which is close enough (in the Hausdorff metric).*

In particular, the theorem states that a thresholding algorithm consistent with a surface tension whose Wulff shape is not a zonoid has to entail convolution with a kernel K that is not positive everywhere, thereby violating the comparison principle that holds for two-phase weighted mean curvature flows. The flows corresponding to such anisotropies cannot even be approximated by threshold dynamics using positive convolution kernels, no matter what mobility one is willing to live with. See Figure 1.

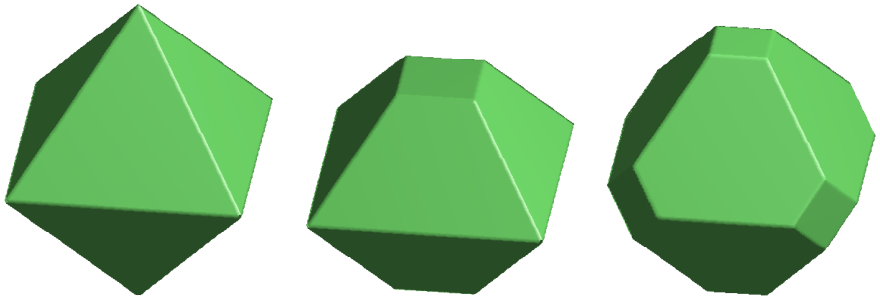

Figure 1: Some non-zonoids. Upshot: A threshold dynamics algorithm of the form (12) & (13) cannot be monotone for any isotropy the Wulff shape of which is close enough to one of these.

Proof. Let $\sigma : \mathbb{S}^2 \to \mathbb{R}$ be a surface tension such that W_σ is not a zonoid. Then there exists a neighborhood $\mathcal{N}$ of W_σ with respect to the Hausdorff distance that contains no zonotopes. Let K be a convolution kernel that is positive. By Proposition 6, algorithm (12) & (13) is consistent with the evolution law (6) for the surface tension & mobility pair given by (26) & (29), and by Proposition 1, only for that pair. We have

$$\sigma_K(n) = \int_{\mathbb{S}^2} |n \cdot x| \, \frac{1}{2} \int_0^\infty K(rx) r^d \, dr \, dH^{d-1}(x).$$

Thus,

$$\omega(x) = \frac{1}{2} \int_0^\infty K(rx) r^d \, dr \geq 0$$

is the generating distribution of σ_K. By Theorem 8, W_{σ_K} is then a zonoid. It is therefore, by definition, the limit of a sequence of zonotopes in the Hausdorff metric. Hence, $W_{\sigma_K} \notin \mathcal{N}$. □

Remark 10. Theorem 9 implies that a construction as general as the one given in Bonnetier et. al. in [6], which works for all anisotropies in three dimensions, could not possibly preserve the comparison principle for the flow in general. This is a limitation on thresholding schemes (12) & (13), regardless of the construction used for the kernel. In light of this limitation, it is interesting to compare threshold dynamics with the nonlinear diffusion generated motion scheme considered by Chambolle and Novaga in [7], which preserves the comparison principle for any anisotropy, at the expense of solving a *nonlinear* diffusion equation at every time step (alternated with thresholding). It appears that if one insists on using just a convolution to do the diffusion step (which is of course much faster), one has to give up something, namely monotonicity, in certain cases in three dimensions.

We now turn to our new method of constructing convolution kernels. The goal is to see whether kernels that are positive in both the physical and Fourier

domains can be found for the anisotropies not ruled out by the barrier Theorem 9 above, i.e. for anisotropies whose Wulff shapes are zonoids. Towards that goal, our idea is to write the kernels as a *sum* of one dimensional Gaussians:

$$g_v(x) := \frac{1}{\sqrt{4\pi}} \exp\left(-\frac{(x\cdot v)^2}{4}\right) \delta\left(|x|^2 - (x\cdot v_i)^2\right) \tag{48}$$

where $v \in \mathbb{S}^{d-1}$ is the direction of diffusion involved in convolutions with (48). In practice, the δ-function in (48) will need to be regularized – for one thing, the mobility of (48) otherwise turns out to be 0. Instead, we will take

$$g_{v,\varepsilon}(x) = \frac{\varepsilon^{1-d}}{(4\pi)^{\frac{d}{2}}} \exp\left(-\frac{(x\cdot v)^2}{4}\right) \exp\left(\frac{(x\cdot v)^2 - |x|^2}{4\varepsilon^2}\right) \tag{49}$$

with the Fourier transform

$$\widehat{g}_{v,\varepsilon}(\xi) = \exp\left(-(v\cdot\xi)^2\right) \exp\left(\varepsilon^2\left((v\cdot\xi)^2 - |\xi|^2\right)\right) \tag{50}$$

where $\varepsilon > 0$. According to e.g. (34) & (33), the corresponding surface tension and mobility are:

$$\sigma_{v,\varepsilon}(n) = \frac{1}{\sqrt{\pi}}\sqrt{(1-\varepsilon^2)(v\cdot n)^2 + \varepsilon^2}$$
$$\mu_{v,\varepsilon}(n) = 2\sqrt{\pi}\sqrt{(1-\varepsilon^2)(v\cdot n)^2 + \varepsilon^2}$$

It is apparent from these formulas that in the limit $\varepsilon \to 0^+$

$$\sigma_{v,\varepsilon}(n) \to \frac{1}{\sqrt{\pi}}\,|v\cdot n| \text{ and } \mu_{v,\varepsilon}(n) \to 2\sqrt{\pi}\,|v\cdot n| \tag{51}$$

uniformly. Summing over directions $v \in \mathbb{S}^{d-1}$ with weight function $\omega : \mathbb{S}^{d-1} \to \mathbb{R}$, we are led to consider kernels of the form

$$K_\varepsilon(x) = \int_{\mathbb{S}^{d-1}} \omega(v) g_{v,\varepsilon}(x)\, dH^{d-1}(v). \tag{52}$$

with Fourier transforms

$$\widehat{K}_\varepsilon(\xi) = \int_{\mathbb{S}^{d-1}} \omega(v) \widehat{g}_{v,\varepsilon}(\xi)\, dH^{d-1}(v). \tag{53}$$

Summing also $\sigma_{v,\varepsilon}$ over all directions v, we get

$$\sigma_\varepsilon(n) = \frac{1}{\sqrt{\pi}} \int_{\mathbb{S}^{d-1}} \omega(v)\sqrt{(1-\varepsilon^2)(v\cdot n)^2 + \varepsilon^2}\, dH^{d-1}(v).$$

Given a desired surface tension $\sigma : \mathbb{S}^{d-1} \to \mathbb{R}$, we can solve the integral equation

$$\sigma(n) = \frac{1}{\sqrt{\pi}} \int_{\mathbb{S}^{d-1}} \omega(v)\,|v\cdot n|\, dH^{d-1}(v) = \frac{1}{\sqrt{\pi}} T\omega \tag{54}$$

for the generating function ω where, we recall, T denotes the cosine transform from Section 5.1. This allows us to express the weight function ω as

$$\omega = \sqrt{\pi}\, T^{-1}\sigma. \tag{55}$$

By Theorem 8, $T^{-1}\sigma$ is smooth if σ is. As long as W_σ is a zonoid, the generating function ω of σ, determined by (55), will be positive. Substituting into (52) we get:

$$K_\varepsilon(x) = \sqrt{\pi} \int_{\mathbb{S}^{d-1}} \left(T^{-1}\sigma\right) g_{v,\varepsilon}(x)\, dH^{d-1}(v) \tag{56}$$

for our kernel, and

$$\widehat{K}_\varepsilon(\xi) = \sqrt{\pi} \int_{\mathbb{S}^{d-1}} \left(T^{-1}\sigma\right) \widehat{g}_{v,\varepsilon}(\xi)\, dH^{d-1}(v) \tag{57}$$

for its Fourier transform. Both K_ε and $\widehat{K}_\varepsilon$are then positive by construction as long as W_σ is a zonoid. Moreover, by (51), for the corresponding surface tension σ_ε we have

$$\sigma_\varepsilon(n) = \int_{\mathbb{S}^{d-1}} \left(T^{-1}\sigma\right) \sqrt{(1-\varepsilon^2)(v\cdot n)^2 + \varepsilon^2}\, dH^{d-1}(v) \to \sigma(n) \tag{58}$$

uniformly as $\varepsilon \to 0^+$, provided that $\sigma(n)$ is a smooth function.

Thus, we see that for any smooth anisotropy the Wulff shape of which is a zonoid, flow (6) can be approximated by threshold dynamics using a convolution kernel that is *positive in both the physical and Fourier domain*, for some choice of non-vanishing (albeit possibly quite complicated) mobility. Since in two dimensions all centrally symmetric convex bodies are zonoids, this in particular includes all two dimensional anisotropies, as can also be seen from the explicit inversion formula (38) for the cosine transform on the circle. In terms of the given anisotropy σ, the mobility of kernel (56) can be expressed as

$$\mu_\varepsilon(n) = \left(\int_{\mathbb{S}^{d-1}} \left(T^{-1}\sigma\right) \frac{1}{\sigma_{v,\varepsilon}(v)}\, dH^{d-1}(v) \right)^{-1}, \tag{59}$$

i.e. it is a weighted harmonic mean of mobilities of the one dimensional kernels, and thus rarely the natural mobility corresponding to the anisotropy σ_ε. We repeat, however, that modifying mobilities in threshold dynamics schemes is relatively easy; see [8] for an example utilizing retardation terms in the variational formulation (21) that leads to a slightly modified version of the basic algorithm (12) & (13). Whether a given anisotropy and mobility pair can be achieved in one shot, by a clever choice of a convolution kernel enjoying desirable positivity properties, and without having to modify algorithm (12) & (13) at all, is an intriguing question that will be addressed elsewhere.

Specializing from now on to $d = 3$ for convenience, alternative forms for expressions (56) & (57) can be obtained via (55) and by recalling property (39) of the cosine transform T :

$$\omega = T^{-1}\sigma = \mathcal{J}_s^{-1}(\Delta_{\mathbb{S}^2} + 2Id)\sigma = (\Delta_{\mathbb{S}^2} + 2Id)\mathcal{J}_s^{-1}\sigma.$$

We get

$$K_\varepsilon(x) = \sqrt{\pi} \int_{\mathbb{S}^2} (\Delta_{\mathbb{S}^2} + 2Id)\, \sigma\, \mathcal{J}_s^{-1} g_{v,\varepsilon}(x)\, dH^2(v)$$
$$= \sqrt{\pi} \int_{\mathbb{S}^2} \sigma\, T^{-1} g_{v,\varepsilon}(x)\, dH^2(v) \tag{60}$$

and

$$\widehat{K}_\varepsilon(\xi) = \sqrt{\pi} \int_{\mathbb{S}^2} (\Delta_{\mathbb{S}^2} + 2Id)\, \sigma\, \mathcal{J}_s^{-1} \widehat{g}_{v,\varepsilon}(\xi)\, dH^2(v)$$
$$\sqrt{\pi} \int_{\mathbb{S}^2} \sigma\, T^{-1} \widehat{g}_{v,\varepsilon}(\xi)\, dH^2(v). \tag{61}$$

Formulas (60) & (61) will be more useful if we can calculate the inverse spherical Radon transforms $\mathcal{J}_s^{-1} g_{v,\varepsilon}$ and $\mathcal{J}_s^{-1} \widehat{g}_{v,\varepsilon}$ of $g_{v,\varepsilon}$ and $\widehat{g}_{v,\varepsilon}$. For either task, the key is to first consider the spherical Radon transform of *radially symmetric* even functions $f : \mathbb{S}^2 \to \mathbb{R}$, i.e. $f = f(\phi)$ where ϕ is the polar angle. Such functions remain so under the spherical Radon transform:

$$\mathcal{J}_s : \left\{ f : \mathbb{S}^2 \to \mathbb{R} \,:\, f = f(\phi) \right\} \to \left\{ f : \mathbb{S}^2 \to \mathbb{R} \,:\, f = f(\phi) \right\}.$$

Moreover, $\mathcal{J}_s$ is known to simplify considerably when restricted to such functions:

$$\mathcal{J}_s f(\arcsin x) = \frac{2}{\pi} \int_0^x \frac{f(\arccos z)}{\sqrt{x^2 - z^2}}\, dz.$$

This is the Abel equation, a standard Volterra integral equation of the first kind, the inversion of which can be accomplished e.g. by the Laplace transform. One gets:

$$f(\arccos z) = \mathcal{J}_s f(0) + z \int_0^z \frac{(\mathcal{J}_s f(\arcsin x))'}{\sqrt{z^2 - x^2}}\, dx. \tag{62}$$

We can now apply (62) to calculate $\mathcal{J}_s^{-1} g_{v,\varepsilon}$ and $\mathcal{J}_s^{-1} \widehat{g}_{v,\varepsilon}$. Starting with $\mathcal{J}_s^{-1} g_{v,\varepsilon}$, take $x = a(0,0,1)$ for some $a \in \mathbb{R}$, thus pointing in the north pole direction. Set

$$\psi(v) := g_{v,\varepsilon}(0,0,a) = \frac{1}{\varepsilon^2 (4\pi)^{3/2}} \exp\left(-\frac{|x|^2}{4\varepsilon^2} \right) \exp\left(\gamma^2 v_3^2 \right)$$

where $\gamma^2 = \frac{|x|^2(1-\varepsilon^2)}{4\varepsilon^2}$. $\psi(v)$ then depends only on $\cos\phi = v_3$ and is thus a radial function. Taking $\mathcal{J}_s f(\phi) = \exp\left(\gamma^2 \cos^2\phi\right)$, we apply (62) to get

$$f(\phi) = \mathcal{J}_s^{-1} \exp\left(\gamma^2 \cos^2\phi\right) = e^{\gamma^2} \left\{ 1 - 2\gamma\, \cos\phi\, D(\gamma \cos\phi) \right\}$$

where the function $D : \mathbb{R} \to \mathbb{R}$ is defined as

$$D(x) = e^{-x^2} \int_0^x e^{y^2}\, dy.$$

Thus,

$$\mathcal{J}_s^{-1}\psi(v) = \frac{1}{\varepsilon^2\,(4\pi)^{\frac{3}{2}}}\exp\left(-\frac{|x|^2}{4}\right)\left\{1-\frac{\sqrt{1-\varepsilon^2}}{\varepsilon}\,|x|\,v_3 D\left(\frac{\sqrt{1-\varepsilon^2}}{2\varepsilon}\,|x|\,v_3\right)\right\}.$$

After a rotation, this implies

$$\mathcal{J}_s^{-1}g_{v,\varepsilon}(x) = \frac{1}{\varepsilon^2\,(4\pi)^{\frac{3}{2}}}\exp\left(-\frac{|x|^2}{4}\right)\left\{1-\frac{\sqrt{1-\varepsilon^2}}{\varepsilon}\;(x\cdot v)\;D\left(\frac{\sqrt{1-\varepsilon^2}}{2\varepsilon}(x\cdot v)\right)\right\}. \quad (63)$$

Turning to the calculation of $\mathcal{J}_s^{-1}\widehat{g}_{v,\varepsilon}$, now set

$$\psi(v) = \widehat{g}_{v,\varepsilon}(0,0,a) = \exp\left(-\varepsilon^2\,|\xi|^2\right)\exp\left(-\gamma^2 v_3^2\right)$$

where $\gamma^2 = (1-\varepsilon^2)\,|\xi|^2$. As before, $\psi(v)$ depends only on $v_3 = \cos\phi$ and is thus radial. Taking $\mathcal{J}_s f(\phi) = \exp\left(\gamma^2\cos^2\phi\right)$ and applying (62), this time we get

$$f(\phi) = \mathcal{J}_s^{-1}\exp\left(-\gamma^2\cos^2\phi\right) = e^{-\gamma^2}\left\{1+\sqrt{\pi}\,\gamma\,\cos\phi\,\mathrm{erf}\left(\gamma\cos\phi\right)\,e^{\gamma^2\cos^2\phi}\right\}$$

where erf denotes the error function. After a rotation, this implies

$$\mathcal{J}_s^{-1}\widehat{g}_{v,\varepsilon}(\xi) = e^{-|\xi|^2}\left\{1+\sqrt{\pi(1-\varepsilon^2)}\,(\xi\cdot v)\,\mathrm{erf}\left(\sqrt{1-\varepsilon^2}(\xi\cdot v)\right)\,e^{\left(1-\varepsilon^2\right)(\xi\cdot v)^2}\right\}. \quad (64)$$

We now explore consequences of (63) & (64).

When W_σ is not a zonoid, we cannot expect construction (52) to allow approximation of flow (6) with a positive kernel: no construction can, according to the barrier Theorem 9 (regardless of the mobility). The monotonicity of scheme (12) & (13) is therefore inevitably lost in these cases. An interesting question is whether the energy dissipation property noted in Proposition 2, which depends on positivity in the Fourier domain, still holds, even for non-zonoidal anisotropies in three dimensions. (Recall that this is the case for the kernels of Bonnetier et. al. by construction, see Section 5.3). We can investigate this question using (61) and (64). First, note that

$$(\Delta_{\mathbb{S}^2} + 2Id)\sigma = \Delta_{\mathbb{R}^3}\sigma \geq 0 \quad (65)$$

by convexity of the one-homogeneous function σ. Next, we observe that (64) implies

$$\mathcal{J}_s^{-1}\widehat{g}_{v,\varepsilon}(\xi) \geq 0$$

for all ξ. Therefore:

$$\widehat{K}_\varepsilon(\xi) = \sqrt{\pi} \int_{\mathbb{S}^2} \underbrace{\mathcal{J}_s^{-1} \widehat{g}_{v,\varepsilon}(\xi)}_{\geq 0 \text{ by (64)}} \underbrace{(\Delta_{\mathbb{S}^2} + 2Id)\sigma}_{\geq 0 \text{ by (65)}} \, dH^2(v)$$
$$\geq 0.$$

Thus, we see that construction (52) always yields convolution kernels that are positive in the Fourier domain, regardless of the dimension and anisotropy σ. The resulting thresholding algorithm (12) & (13) therefore always has the energy dissipation property of Proposition 2. We have established the following theorem that summarizes the foregoing discussion:

Theorem 11. *Threshold dynamics algorithm (12) & (13) can approximate (at the level of consistency) weighted mean curvature motion (6) for a given anisotropy $\sigma : \mathbb{S}^{d-1} \to \mathbb{R}^+$ up to a mobility factor $\mu : \mathbb{S}^{d-1} \to \mathbb{R}^+$ with a positive convolution kernel – thereby preserving the monotonicity of the geometric flow – if and only if the corresponding Wulff shape W_σ of σ is a zonoid. Construction (56) of the convolution kernel is maximally positive, in the sense that the resulting kernel K_ε satisfies:*

1. *$\widehat{K}_\varepsilon(\xi) \geq 0$ for all anisotropies σ, and*
2. *$K_\varepsilon(x) \geq 0$ whenever W_σ is a zonoid.*

Remark 12. The basic result of Theorem 8 on zonoids, and its consequences Theorems 9 and 11, appear to have implications for macroscopic limits of Ising models. Indeed, [24] provides an expression for the continuum surface energy that corresponds to a given lattice model in terms of the interaction strength between neighboring lattice sites. At zero temperature, that expression is a discrete version of (35), with $f(n)$ in (35) playing the role of the bond energy between an atom at the origin and its neighbor located at n. It follows that in the case of *ferromagnetic Ising models*, where all interactions have positive energy, the corresponding Wulff crystal is always a zonoid. In particular, a Wulff shape such as the octahedron can never arise from ferromagnetic Ising models. To put a positive spin on the foregoing discussion, Theorem 11 implies that a thresholding scheme enjoying both monotonicity and energy dissipation properties can be found for any anisotropy arising from a ferromagnetic Ising model; our new kernel construction exhibits one way of doing so.

As an application of (60) & (63), the expression (56) for our convolution kernel, given in terms of the anisotropy σ , can be made more explicit in the case when σ is crystalline (i.e. B_σ is a polyhedron). Let B_σ be represented as

$$B_\sigma = \bigcap_{i=1}^{M} h(n_i, r_i)$$

where $h(n_i, r_i) = \left\{x \in \mathbb{R}^3 \, : \, x \cdot n_i =\leq r\right\}$ so that $n_i \in \mathbb{S}^2$ are the unit outward normals to the faces of ∂B_σ and and $r_i \in \mathbb{R}$ are the distances of $\partial h(n_i, r_i)$ to

the origin. Enumerate the edges of ∂B_σ as $\ell_{i,j} = \partial h(n_i, r_i) \cap \partial h(n_j, r_j) \cap \partial B_\sigma$, some of which are possibly empty. Let $P : \mathbb{R}^3 \setminus \{0\} \to \mathbb{S}^2$ denote the projection $P(x) = \frac{x}{|x|}$. Then, on $\mathbb{S}^2$ we have

$$(\Delta_{\mathbb{S}^2} + 2Id)\,\sigma = \sum_{i,j} \left| \frac{1}{r_i} n_i - \frac{1}{r_j} n_j \right| \delta_{P\ell_{i,j}}(x) \tag{66}$$

where $\delta_{P\ell_{i,j}}(x)$ denotes a delta function on $\mathbb{S}^2$ along the great circular arc $P\ell_{i,j}$. Using (60) together with (63) and (66), we get the following quite explicit formula:

$$K_\varepsilon(x) = \frac{e^{-\frac{|x|^2}{4}}}{8\pi\varepsilon^2} \sum_{i,j} \left| \frac{n_i}{r_i} - \frac{n_j}{r_j} \right| \int_{P\ell_{i,j}} 1 - \frac{\sqrt{1-\varepsilon^2}}{\varepsilon}\,(x\cdot v)\, D\left(\frac{\sqrt{1-\varepsilon^2}}{\varepsilon}\,(x\cdot v) \right) dH^1(v). \tag{67}$$

See Section 6 for a numerical example where (67) is used to construct the convolution kernel in algorithm (12) & (13).

We conclude our discussion of the new kernel construction with the following comment: (60) implies that explicit formula (67) can be used to construct approximate kernels for smooth anisotropies as well: Once $\varepsilon > 0$ has been chosen small enough so that the corresponding surface tension σ_ε given by (58) approximates the given anisotropy σ well, we may replace σ in (60) by a close enough crystalline approximation at the cost of incurring a small perturbation in K_ε and therefore in its corresponding surface tension. Of course, the multiple levels of approximation entailed in this procedure can be undesirable in practice.

6 Numerical examples

To demonstrate the new kernels (52), we compute the Wulff shape W_σ corresponding to several given anisotropies σ as the stationary state of area or volume preserving weighted mean curvature motion. It is easy to adapt threshold dynamics algorithm (12) & (13) to this evolution, see e.g. [27, 28]:[1]

[1]The authors became aware of Xu, Wang & Wang's work [28] during the preparation of this manuscript, who have independently discovered algorithm (68), (69) & (70) that is a simplification of the one in [27].

Algorithm: Let $M = \#\{i : \mathbf{1}_{\Sigma^0}(x_i) = 1\}$ where x_i are the spatial grid points.

1. Convolution:

$$\psi^k = \frac{1}{(\delta t)^{\frac{d}{2}}} K\left(\frac{x}{\sqrt{\delta t}}\right) * \mathbf{1}_{\Sigma^k} \tag{68}$$

2. Sorting: Set:

$$\alpha(i) = i\text{-th largest } \psi^k(x_i). \tag{69}$$

3. Thresholding:

$$\Sigma^{k+1} = \left\{x : \psi^k(x) \geq \alpha(M)\right\}. \tag{70}$$

Figure 2 shows the results of two-phase numerical experiments in two dimensions for the following surface tensions

$$\begin{aligned}
\sigma(x) &= |x_1| + |x_2|\,, \\
\sigma(x) &= |x_2| + \frac{1}{\sqrt{2}}|x_1 + x_2| + \frac{1}{\sqrt{2}}|x_1 - x_2|\,, \text{ and} \\
\sigma(x) &= |x_1| + |x_2| + \frac{1}{\sqrt{2}}|x_1 + x_2| + \frac{1}{\sqrt{2}}|x_1 - x_2|
\end{aligned}$$

for which the corresponding Wulff shapes are a square, a hexagon, and an octagon, in that order. Since these surface tensions are already in the additive form (54), where the generating distribution ω is a sum of delta masses for each, the corresponding approximate kernels based on our construction are very easy to obtain; they are

$$K_\varepsilon = g_{e_1,\varepsilon} + g_{e_2,\varepsilon}, \tag{71}$$

$$K_\varepsilon = g_{e_2,\varepsilon} + \frac{1}{\sqrt{2}} g_{e_1+e_2,\varepsilon} + \frac{1}{\sqrt{2}} g_{e_1-e_2,\varepsilon}, \text{ and} \tag{72}$$

$$K_\varepsilon = g_{e_1,\varepsilon} + g_{e_2,\varepsilon} + \frac{1}{\sqrt{2}} g_{e_1+e_2,\varepsilon} + \frac{1}{\sqrt{2}} g_{e_1-e_2,\varepsilon} \tag{73}$$

respectively, where $g_{v,\varepsilon}$ is given by (49).

Figure 3 shows a two-phase computation in three dimensions with a kernel K using the new construction, where the corresponding anisotropy $\sigma(x) = \ell^\infty(x) = \max\{|x_1|, |x_2|, |x_3|\}$ has the octahedron (i.e $\ell^1(x) \leq 1$) as its Wulff shape. Recall that since the octahedron is not a zonoid, no consistent kernel can be positive. The new kernel construction method is particularly complicated in this case, as the generating distribution ω given by (55) is not even a signed

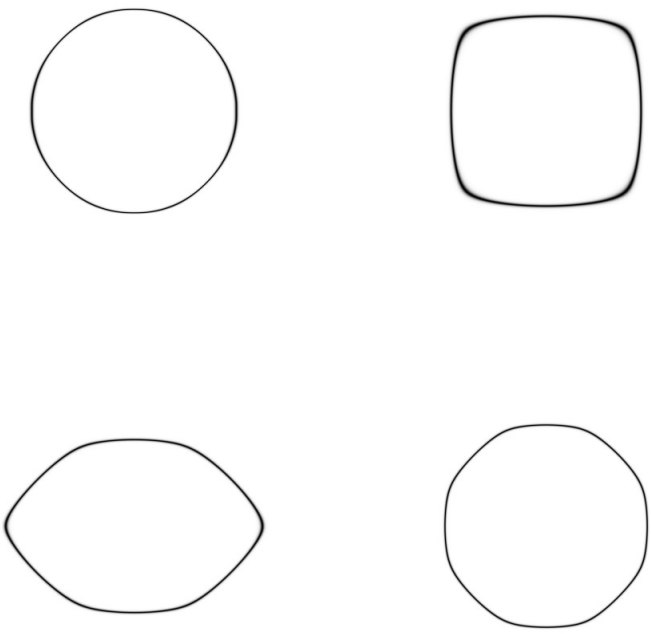

Figure 2: Upper left: Initial interface used in algorithm (68), (69) & (70). Upper right: Stationary state reached with kernel (71) that approximately corresponds to a square Wulff shape. Lower right: Stationary state reached with kernel (72) that approximately corresponds to a hexagonal Wulff shape. Lower right: Stationary state reached with kernel (73) that approximately corresponds to an octagonal Wulff shape.

measure; see Figure 4 for a visualization. Nevertheless, the resulting regularized kernel is easy to express, both in the Fourier and physical domains, thanks to formulas (56) & (57).

The multiphase variational formulation of threshold dynamics and the resulting algorithm given in [8] for isotropic but unequal surface tensions extends immediately to the fully anisotropic, multiphase setting of energy (2). The nonlocal approximate energy – the multiphase version of (20) – is simply

$$E_{\delta t}(\Sigma_1, \dots, \Sigma_N) = \frac{1}{\sqrt{\delta t}} \sum_{\substack{i,j=1 \\ i \neq j}}^{N} \int_{\Sigma_j} K_{\delta t}^{i,j} * \mathbf{1}_{\Sigma_i} \, dx \tag{74}$$

where for each interface $(\partial\Sigma_i) \cap (\partial\Sigma_j)$ in the network we have a different convolution kernel $K^{i,j} = K^{j,i}$ (not required to have unit mass) adapted to the anisotropy $\sigma_{i,j}$ of that interface. The systematic procedure described in [8] that derives a threshold dynamics scheme from such nonlocal approximations yields the following algorithm:

Algorithm: Alternate the following steps:

1. Convolution:
$$\psi_i^k = \sum_{\substack{j=1 \\ j \neq i}}^{N} K_{\delta t}^{i,j} * \mathbf{1}_{\mathbf{\Sigma_j^k}} \tag{75}$$

2. Thresholding:
$$\Sigma_i^{k+1} = \left\{ x \, : \, \psi_i^k(x) = \min_{j \in \{1,2,3,\dots,N\}} \psi_j^k(x) \right\}. \tag{76}$$

Whether algorithm (75) & (76) can be guaranteed to dissipate energy (74) at every step appears to be a challenging question, and will likely require additional assumptions on the convolution kernels. (Even the well posedness of the variational problem (2) itself is complicated at this level of generality, see e.g. [3]). These questions are beyond the scope of the present paper. Here, in the spirit of this numerical section, we will use algorithm (75) & (76), without any rigorous justification, to explore whether the more granular understanding of Ruuth-Merriman kernels afforded by our variational view point, as claimed in Section 5.2, has any merit. As explained there, the discussion in [26] does not distinguish the contribution to the normal speed stemming from the mobility factor vs. the surface tension associated with their anisotropic kernels. The formulas (26) & (29) of Section 4, which were used in Section 5.2 to separately identify the mobility and surface tension factors corresponding to a given Ruuth-Merriman kernel, are particularly useful in the multiphase case of model (2), since the surface tensions of the interfaces meeting at a junction determine the boundary conditions there – their mobilities play no role in it. Figure 5 shows a

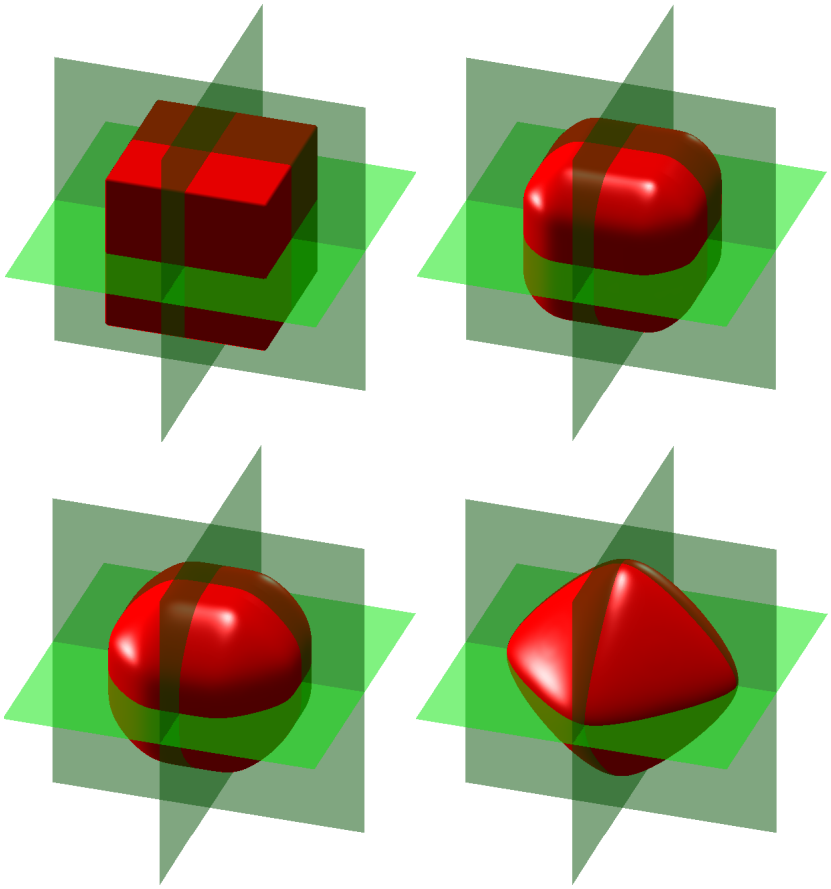

Figure 3: An experiment, on an $128 \times 128 \times 128$ grid, with the new kernel construction for the anisotropy $\sigma(x) = \max\{|x_1|, |x_2|, |x_3|\}$. Since the corresponding Wulff shape is an octahedron, which is not a zonoid, no consistent kernel can be positive. Thus even the new construction method necessarily yields a kernel that changes sign. From left to right and top to bottom: Initial condition, intermediate stages, and final state of evolution via algorithm (68), (69) & (70).

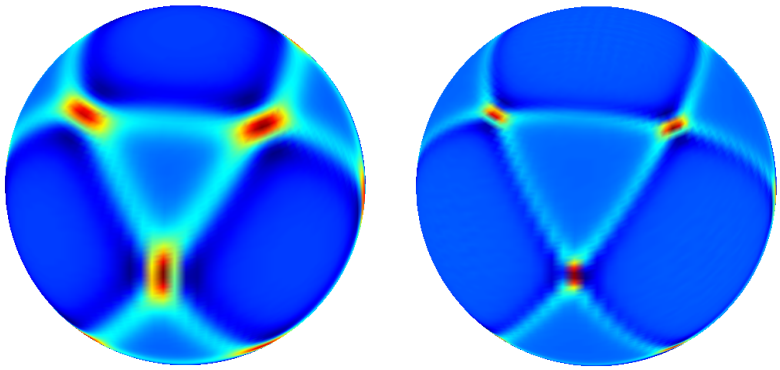

Figure 4: The new kernel construction becomes particularly nontrivial for crystalline anisotropies with non-zonoidal Wulff shapes. Shown here are smooth approximations (less regularized on the right) to the generating distribution ω for the anisotropy $\sigma(x) = \max\{|x_1|, |x_2|, |x_3|\}$ that has an octahedron as its Wulff shape. In this case, ω is not even a signed measure. The approximate kernel K_ε, constructed according to (56) or (57), nevertheless has a smooth and positive Fourier transform.

three-phase computation with algorithm (75) & (76) in which each convolution kernel is taken to be

$$K(x) = \mathbf{1}_\Omega(x) \tag{77}$$

where Ω is the ellipse

$$\Omega = \left\{(x_1, x_2) \in \mathbb{R}^2 \,:\, 3x_1^2 + x_2^2 = 3\right\}. \tag{78}$$

The figure shows the steady state reached starting from an initial condition containing a T-junction (90°, 180°, 90° angles at the junction), using Dirichlet boundary conditions. Since Ω is obtained from a disk by a simple dilation, and since threshold dynamics using the characteristic function of a disk as the convolution kernel has as its stationary state triple junctions with 120° angles, it immediately follows that a configuration of three straight interfaces having e_1, $\frac{1}{\sqrt{2}}(e_1, e_2)$, and $\frac{1}{\sqrt{2}}(-e_1, e_2)$ as their normals and meeting at a $(135°, 90°, 135°)$ triple junction is stationary under algorithm (75) & (76) if all $K^{i,j}$ are taken to be (77). This is consistent with formula (26): Indeed, we have

$$R(\theta) = \frac{\sqrt{3}}{\sqrt{2\cos^2\theta + 1}}$$

which by (45) corresponds to the surface tension

$$\sigma(\theta) = 4\sqrt{1 - \frac{2}{3}\cos^2\theta}.$$

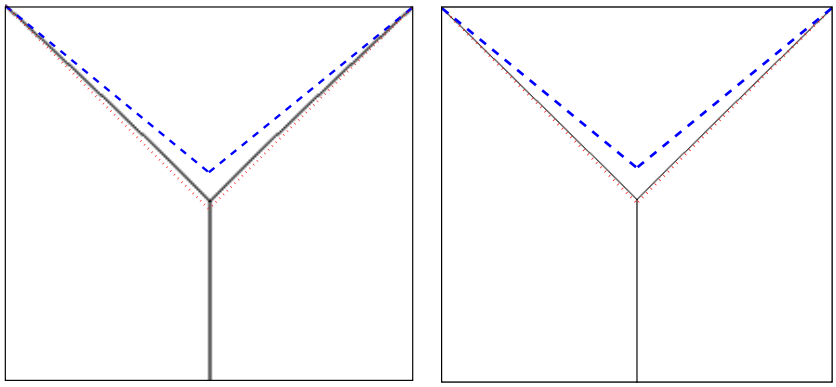

Figure 5: Stationary state reached by Algorithm (75) & (76) using the anisotropic convolution kernel (77) & (78) on three phases, subject to Dirichlet boundary conditions. The solid lines are the computed steady state. The blue dashed line is the steady state predicted by the naive interpretation of Ruuth & Merriman's kernel construction that does not distinguish between contributions to the normal speed of an interface stemming from the mobility vs. the surface tension factors. The red dotted line is the predicted steady state by our energetic interpretation that identifies, separately, the mobility and surface tension that correspond to a given kernel. The left figure was computed on a 256×256 grid, and the right figure on a 512×512 one.

The junction condition (8) can now be used, along with symmetry considerations, to infer that with this surface tension the angles at the junction should in fact be $(135°, 90°, 135°)$, as is observed in the numerical experiment.

On the other hand, the normal speed generated by the scheme is

$$v_\perp = (f'' + f)\,\kappa \text{ with}$$
$$f(\theta) = 2\sqrt{6}\,\cos\theta \operatorname{arctanh}\left(\sqrt{\frac{2}{3}}\cos\theta\right) + 6\sqrt{2}\,\sin\theta\,\arctan\left(\sqrt{2}\sin\theta\right).$$

Mistakingly interpreting f in this formula as the surface tension leads to predicted junction angles of approximately $(129.4°, 101.3°, 129.4°)$, also shown in Figure 5 for comparison.

7 Appendix

In this section, we verify that assumptions (14), (15), (16) & (17) on the convolution kernel K are sufficient to endow scheme (12) & (13) with a very basic level of consistency with the evolution law (6), in the sense that one step of the algorithm, acting on a set with smooth boundary, generates the advertised normal speed to leading order in δt . This elementary calculation, essentially a

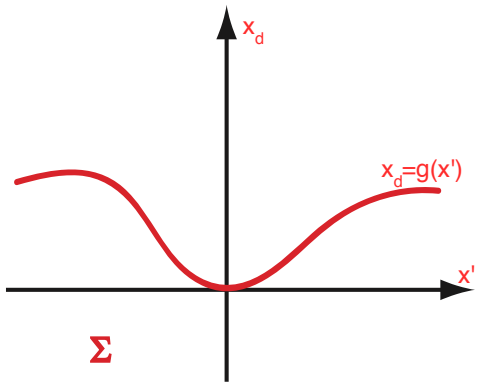

Figure 6: Set up used in consistency calculation.

Taylor expansion, has already been carried out multiple times in existing literature under various assumptions on the convolution kernel K. For the sake of completeness, and because our assumptions on the kernel are slightly different than in previous papers, we include the derivation below.

Proposition 13. *For a kernel satisfying assumptions (15), (16), and (17), threshold dynamics algorithm (12) & (13) is consistent with the normal speed*

$$v_n(x) = \frac{1}{2\int_{n^\perp(x)} K(y)\, dH^{d-1}(y)} \int_{n^\perp(x)} \left[\kappa_1 (v_1 \cdot y)^2 + \kappa_2 (v_2 \cdot y)^2\right] K(y)\, dH^{d-1}(y)$$

where v_1 & v_2 are the principal curvature directions and κ_1 & κ_2 are the corresponding principal curvatures of $\partial\Sigma$ at x, in the sense that for a compact set Σ with smooth boundary $\partial\Sigma$, we have

$$\begin{aligned} K_{\delta t} * \mathbf{1}_\Sigma (x + sn(x)) = \frac{1}{2} &- \frac{s}{\sqrt{\delta t}} \int_{n^\perp(x)} K(y)\, dH^{d-1}(y) \\ &+ \sqrt{\delta t} \int_{n^\perp(x)} \left[\kappa_1 (v_1 \cdot y)^2 + \kappa_2 (v_2 \cdot y)^2\right] K(y)\, dH^{d-1}(y) \\ &+ o(\sqrt{\delta t}) \end{aligned} \tag{79}$$

as $\delta t \to 0$, where $n(x)$ is the outward unit normal to $\partial\Sigma$ at x.

Remark 14. Setting (79) equal to $\frac{1}{2}$ and solving for s using assumption (17), we see that if expansion (79) can be verified for a given kernel K, then at the end of a time step taken with scheme (12) & (13), the new interface will contain the point $x + s_* n(x)$ where $s_* = v_n(x)\delta t + o(\delta t)$

Proof. Let $\Sigma \subset \mathbb{R}^d$ be a compact set with smooth boundary $\partial\Sigma$. Let $n(p)$ denote the unit outward normal to Σ at $p \in \partial\Sigma$. Let $\mathcal{O}$ be an orthogonal, $d \times d$ matrix such that $\mathcal{O}e_d = n(p)$. Let $T : \mathbb{R}^d \to \mathbb{R}^d$ be the affine map $Tx = \mathcal{O}x + p$. Then,

$\partial(T^{-1}\Sigma)$ is given as the graph of a smooth function $g : \mathbb{R}^{d-1} \to \mathbb{R}$ in a small enough neighborhood $|x| \le r$ of 0 such that

$$g(0) = 0 \text{ and } \nabla g(0) = 0.$$

Moreover, e_d is the outward unit normal to $\partial(T^{-1}\Sigma)$ at 0. Extend g to all $\mathbb{R}^{d-1}$ so that it and its first three derivatives remain bounded, and let $\tilde{\Sigma} = \left\{x = (x', x_d) \in \mathbb{R}^d \,:\, x_d \le g(x')\right\}$. Let us write $\varepsilon = \sqrt{\delta t}$ for convenience, and let $\tilde{K} = K \circ \mathcal{O}$. We have

$$\begin{aligned}
\left(K_{\varepsilon^2} * \mathbf{1}_\Sigma\right)(p + sn(p)) &= \left(\tilde{K}_{\varepsilon^2} * \mathbf{1}_{T^{-1}\Sigma}\right)(se_d) \\
&= \int_{\mathbb{R}^d} \tilde{K}_{\varepsilon^2}(se_d - \mathbf{x})\, \mathbf{1}_{T^{-1}\Sigma}(\mathbf{x})\, d\mathbf{x} \\
&= \int_{\mathbb{R}^d} \tilde{K}_{\varepsilon^2}(se_d - \mathbf{x})\, \mathbf{1}_{\tilde{\Sigma}}(\mathbf{x})\, d\mathbf{x} + o(\varepsilon)
\end{aligned}$$

for $|s| \le \frac{r}{2}$ as $\varepsilon \to 0$, where we observed that

$$\left|\int_{\mathbb{R}^d} \tilde{K}_{\varepsilon^2}(se_d - \mathbf{x})\left(\mathbf{1}_{T^{-1}\Sigma}(\mathbf{x}) - \mathbf{1}_{\tilde{\Sigma}}(\mathbf{x})\right)\, d\mathbf{x}\right| \le \int_{|\mathbf{x}| \ge r} \left|\tilde{K}_{\varepsilon^2}(se_d - \mathbf{x})\right|\, d\mathbf{x} = o(\varepsilon)$$

by (19). For the remaining term, we have

$$\int_{\mathbb{R}^d} \tilde{K}_{\varepsilon^2}(se_d - \mathbf{x})\, \mathbf{1}_{\tilde{\Sigma}}(\mathbf{x})\, d\mathbf{x} = \int_{\mathbb{R}^{d-1}} \int_{-\infty}^{g(\mathbf{x}')} \tilde{K}_{\varepsilon^2}(\mathbf{x}', s - \mathbf{x}_d)\, d\mathbf{x}_d\, d\mathbf{x}'.$$

Making the change of variables

$$\bar{\mathbf{x}}' = \frac{\mathbf{x}'}{\varepsilon}\ ,\ \bar{\mathbf{x}}_d = \frac{\mathbf{x}_d}{\varepsilon} \text{ so that } \bar{\mathbf{x}} = \frac{\mathbf{x}}{\varepsilon}\ ,\ \text{and } \bar{z} = \frac{s}{\varepsilon^2}$$

we get

$$\begin{aligned}
\int_{\mathbb{R}^d} \tilde{K}_{\varepsilon^2}(se_d - \mathbf{x})\, \mathbf{1}_{\tilde{\Sigma}}(\mathbf{x})\, d\mathbf{x} &= \int_{\mathbb{R}^{d-1}} \int_{-\infty}^{\frac{1}{\varepsilon} g(\varepsilon \bar{\mathbf{x}}')} \tilde{K}(\bar{\mathbf{x}}', \varepsilon\bar{z} - \bar{\mathbf{x}}_d)\, d\bar{\mathbf{x}}_d\, d\bar{\mathbf{x}}'. \\
&= \int_{\mathbb{R}^{d-1}} \int_{-\infty}^{0} + \int_{\mathbb{R}^{d-1}} \int_{0}^{\frac{\varepsilon}{2}\langle D^2 g(0)\bar{\mathbf{x}}', \bar{\mathbf{x}}'\rangle} + \int_{\mathbb{R}^{d-1}} \int_{\frac{\varepsilon}{2}\langle D^2 g(0)\bar{\mathbf{x}}', \bar{\mathbf{x}}'\rangle}^{\frac{1}{\varepsilon} g(\varepsilon \bar{\mathbf{x}}')} \\
&= (I) + (II) + (III).
\end{aligned}$$

Let $\gamma > 0$ be as in (19). Since g is smooth, we have

$$\left|\frac{1}{\varepsilon} g(\varepsilon \bar{\mathbf{x}}') - \frac{\varepsilon}{2}\langle D^2 g(0)\bar{\mathbf{x}}', \bar{\mathbf{x}}'\rangle\right| \le C' \varepsilon^{1+\gamma} \left|\bar{\mathbf{x}}'\right|^2 \tag{80}$$

for $|\bar{\mathbf{x}}'| \leq \varepsilon^{\gamma-1}$ and some constant $C' \geq 0$. Thus:

$$
\begin{aligned}
|(III)| &\leq \int_{\mathbb{R}^{d-1}} \int_{\frac{\varepsilon}{2}\langle D^2 g(0)\bar{\mathbf{x}}',\bar{\mathbf{x}}'\rangle}^{\frac{1}{\varepsilon}g(\varepsilon\bar{\mathbf{x}}')} \left|\tilde{K}(\bar{\mathbf{x}}', \varepsilon\bar{z} - \bar{\mathbf{x}}_d)\right| \, d\bar{\mathbf{x}}_d \, d\bar{\mathbf{x}}' \qquad (81)\\
&= \int_{|\bar{\mathbf{x}}'|\leq\varepsilon^{\gamma-1}} \int_{\frac{\varepsilon}{2}\langle D^2 g(0)\bar{\mathbf{x}}',\bar{\mathbf{x}}'\rangle}^{\frac{1}{\varepsilon}g(\varepsilon\bar{\mathbf{x}}')} \left|\tilde{K}(\bar{\mathbf{x}}', \varepsilon\bar{z} - \bar{\mathbf{x}}_d)\right| \, d\bar{\mathbf{x}}_d \, d\bar{\mathbf{x}}' + o(\varepsilon) \text{ (by (19))}\\
&\leq \int_{|\bar{\mathbf{x}}'|\leq\varepsilon^{\gamma-1}} \int_{\frac{\varepsilon}{2}\langle D^2 g(0)\bar{\mathbf{x}}',\bar{\mathbf{x}}'\rangle - C'\varepsilon^{1+\gamma}|\bar{\mathbf{x}}'|^2}^{\frac{\varepsilon}{2}\langle D^2 g(0)\bar{\mathbf{x}}',\bar{\mathbf{x}}'\rangle + C'\varepsilon^{1+\gamma}|\bar{\mathbf{x}}'|^2} \left|\tilde{K}(\bar{\mathbf{x}}', \varepsilon\bar{z} - \bar{\mathbf{x}}_d)\right| \, d\bar{\mathbf{x}}_d \, d\bar{\mathbf{x}}'\\
&\quad + o(\varepsilon) \text{ (by (80))}\\
&\leq 2C'\varepsilon^{1+\gamma} \int_{\mathbb{R}^{d-1}} \frac{C}{1+|\bar{\mathbf{x}}'|^p} \, d\bar{\mathbf{x}}' + o(\varepsilon) \text{ (by (14))}\\
&= o(\varepsilon).
\end{aligned}
$$

For (I), we have

$$
\begin{aligned}
(I) &= \int_{\mathbb{R}^{d-1}} \int_{-\infty}^{0} \tilde{K}(\bar{\mathbf{x}}', \varepsilon\bar{z} - \bar{\mathbf{x}}_d) \, d\bar{\mathbf{x}}_d \, d\bar{\mathbf{x}}'\\
&= \int_{\varepsilon\bar{z}}^{\infty} \int_{\mathbb{R}^{d-1}} \tilde{K}(\bar{\mathbf{x}}', \bar{\mathbf{y}}) \, d\bar{\mathbf{x}}' \, d\bar{\mathbf{y}}\\
&= \frac{1}{2} - \int_{0}^{\varepsilon\bar{z}} \int_{\mathbb{R}^{d-1}} \tilde{K}(\bar{\mathbf{x}}', \bar{\mathbf{y}}) \, d\bar{\mathbf{x}}' \, d\bar{\mathbf{y}}
\end{aligned}
$$

The function

$$\xi \to \int_{\mathbb{R}^{d-1}} \tilde{K}(\bar{\mathbf{x}}', \xi) \, d\bar{\mathbf{x}}'$$

has $\xi = 0$ as a point of continuity according to (18). Therefore:

$$\int_{0}^{\varepsilon\bar{z}} \int_{\mathbb{R}^{d-1}} \tilde{K}(\bar{\mathbf{x}}', \bar{\mathbf{y}}) \, d\bar{\mathbf{x}}' \, d\bar{\mathbf{y}} = \varepsilon\bar{z} \int_{\mathbb{R}^{d-1}} \tilde{K}(\bar{\mathbf{x}}', 0) \, d\bar{\mathbf{x}}' + o(\varepsilon).$$

This gives

$$(I) = \frac{1}{2} - \varepsilon\bar{z} \int_{\mathbb{R}^{d-1}} \tilde{K}(\bar{\mathbf{x}}', 0) \, d\bar{\mathbf{x}}' + o(\varepsilon). \qquad (82)$$

For (II), we have

$$
\begin{aligned}
(II) &= \int_{\mathbb{R}^{d-1}} \int_{0}^{\frac{\varepsilon}{2}\langle D^2 g(0)\bar{\mathbf{x}}',\bar{\mathbf{x}}'\rangle} \tilde{K}(\bar{\mathbf{x}}', \varepsilon\bar{z} - \bar{\mathbf{x}}_d) \, d\bar{\mathbf{x}}_d \, d\bar{\mathbf{x}}'\\
&= \varepsilon \int_{0}^{1} \int_{\mathbb{R}^{d-1}} \tilde{K}\left(\bar{\mathbf{x}}', \varepsilon\left[\bar{z} - \bar{\mathbf{y}}\langle D^2 g(0)\bar{\mathbf{x}}', \bar{\mathbf{x}}'\rangle\right]\right) \langle D^2 g(0)\bar{\mathbf{x}}', \bar{\mathbf{x}}'\rangle \, d\bar{\mathbf{x}}' \, d\bar{\mathbf{y}}\\
&\quad \text{(changed variables: } \bar{\mathbf{x}}_d = \tfrac{\varepsilon}{2}\langle D^2 g(0)\bar{\mathbf{x}}', \bar{\mathbf{x}}'\rangle\bar{\mathbf{y}}) \ .
\end{aligned}
$$

By (16) we have

$$\int_{\mathbb{R}^{d-1}} \tilde{K}\left(\bar{\mathbf{x}}', \varepsilon\left[\bar{z} - \bar{\mathbf{y}}\langle D^2 g(0)\bar{\mathbf{x}}', \bar{\mathbf{x}}'\rangle\right]\right)\langle D^2 g(0)\bar{\mathbf{x}}', \bar{\mathbf{x}}'\rangle \, d\bar{\mathbf{x}}' \\ \longrightarrow \int_{\mathbb{R}^{d-1}} \tilde{K}(\bar{\mathbf{x}}', 0)\langle D^2 g(0)\bar{\mathbf{x}}', \bar{\mathbf{x}}'\rangle \, d\bar{\mathbf{x}}'$$

for every $\bar{\mathbf{y}} \in [0,1]$ as $\varepsilon \to 0$, and by (15),

$$\left|\int_{\mathbb{R}^{d-1}} \tilde{K}\left(\bar{\mathbf{x}}', \varepsilon\left[\bar{z} - \bar{\mathbf{y}}\langle D^2 g(0)\bar{\mathbf{x}}', \bar{\mathbf{x}}'\rangle\right]\right)\langle D^2 g(0)\bar{\mathbf{x}}', \bar{\mathbf{x}}'\rangle \, d\bar{\mathbf{x}}'\right| \\ \leq C \int_{\mathbb{R}^{d-1}} \frac{1}{1 + |\bar{\mathbf{x}}'|^p} \, d\bar{\mathbf{x}}' < \infty.$$

Thus, by dominated convergence, we have:

$$(II) = \frac{\varepsilon}{2} \int_{\mathbb{R}^{d-1}} \tilde{K}(\bar{\mathbf{x}}', 0)\langle D^2 g(0)\bar{\mathbf{x}}', \bar{\mathbf{x}}'\rangle \, d\bar{\mathbf{x}}' + o(\varepsilon). \tag{83}$$

Putting (81), (82), and (83) together, we obtain

$$K_{\delta t} * \mathbf{1}_\Sigma \left(x + sn(x)\right) = \frac{1}{2} - \frac{1}{\sqrt{\delta t}} s \int_{n^\perp(x)} K(y) \, dH^{d-1}(y) \\ + \frac{\sqrt{\delta t}}{2} \int_{n^\perp(x)} K(y)\langle D^2 g(x) y, y\rangle \, dH^{d-1}(y) + o(\sqrt{\delta t}) \tag{84}$$

Because $g(x) = 0$ and $\nabla g(0) = 0$, it follows that v_1 & v_2 are the eigenvectors of $D^2 g(x)$ with κ_1 and κ_2 the corresponding eigenvalues. Writing $y = (v_1 \cdot y)v_1 + (v_2 \cdot y)v_2$, we have

$$D^2 g(x) y = \kappa_1 (v_1 \cdot y) v_1 + \kappa_2 (v_2 \cdot y) v_2$$

and so

$$\left\langle D^2 g(x) y, y \right\rangle = \kappa_1 (v_1 \cdot y)^2 + \kappa_2 (v_2 \cdot y)^2. \tag{85}$$

The proposition follows from (84) & (85). □

8 Acknowledgements

The authors are grateful to Felix Otto for many valuable insights and discussions. Part of the work was carried out during visits to the Max Planck Institute for Mathematics in the Sciences in Leipzig, and Centre de Recherches Mathematiques and McGill University in Montreal. The hospitality of these institutions is gratefully acknowledged. Matt Elsey's work was supported by NSF OISE-0967140. Selim Esedoglu's work was supported by NSF DMS-1317730.

References

[1] G. Alberti and G. Bellettini. A non-local anisotropic model for phase transitions: asymptotic behavior of rescaled energies. *European J. Appl. Math.*, 9:261–284, 1998.

[2] F. Almgren, J. E. Taylor, and L.-H. Wang. Curvature-driven flows: a variational approach. *SIAM Journal on Control and Optimization*, 31(2):387–438, 1993.

[3] L. Ambrosio and A. Braides. Functionals defined on partitions in sets of finite perimeter II: semicontinuity, relaxation, and homogenization. *J. Math. Pures et Appl.*, 69:307–333., 1990.

[4] G. Barles and C. Georgelin. A simple proof of convergence for an approximation scheme for computing motions by mean curvature. *SIAM J. Numer. Anal.*, 32:484–500, 1995.

[5] Ethan D. Bolker. A class of convex bodies. *Transactions of the American Mathematical Society*, 145:323–345, 1969.

[6] E. Bonnetier, E. Bretin, and A. Chambolle. Consistency result for a non-monotone scheme for anisotropic mean curvature flow. *Interfaces and Free Boundaries*, 14(1):1–35, 2012.

[7] A. Chambolle and M. Novaga. Approximation of the anisotropic mean curvature flow. *Mathematical Models and Methods in Applied Sciences*, 17(6):833–844, 2007.

[8] S. Esedoḡlu and F. Otto. Threshold dynamics for networks with arbitrary surface tensions. *Communications on Pure and Applied Mathematics*, 68(5):808–864, 2015.

[9] L. C. Evans. Convergence of an algorithm for mean curvature motion. *Indiana University Mathematics Journal*, 42:553–557, 1993.

[10] Paul Goodey and Wolfgang Weil. Centrally symmetric convex bodies and the spherical Radon transform. *Journal of Differential Geometry*, 35:675–688, 1992.

[11] Sigurdur Helgason. *The Radon Transform*, volume 5 of *Progress in Mathematics*. Birkhauser, Boston, MA, 1999.

[12] C. Herring. *The Physics of Powder Metallurgy*, chapter Surface tension as a motivation for sintering, pages 143–179. McGraw Hill, 1951.

[13] E. A. Holm, G. N. Hassold, and M. A. Miodownik. Dimensional effects on anisotropic grain growth. In G. Gottstein and D. Molodov, editors, *Recrystallization and Grain Growth*, pages 239–244, RWTH Aachen, Germany, August 2001. First Joint International Conference on Recrystallization and Grain Growth, Springer-Verlag.

[14] E. A. Holm, G. N. Hassold, and M. A. Miodownik. On misorientation distribution evolution during anisotropic grain growth. *Acta Materialia*, 49:2981–2991, 2001.

[15] H. Ishii, G. E. Pires, and P. E. Souganidis. Threshold dynamics type approximation schemes for propagating fronts. *Journal of the Mathematical Society of Japan*, 51:267–308, 1999.

[16] D. Kinderlehrer, I. Livshits, G. S. Rohrer, S. Taasan, and P. Yu. Mesoscale simulation of the evolution of the grain boundary character distribution. In *Recrystallization and grain growth. Parts 1 and 2.*, pages 1063–1068, 2004.

[17] T. Laux and F. Otto. Convergence of the thresholding scheme for multi-phase mean-curvature flow. Technical Report 33/2015, Max Planck Institute for Mathematics in the Sciences, 2015.

[18] S. Luckhaus and T. Sturzenhecker. Implicit time discretization for the mean curvature flow equation. *Calculus of Variations and Partial Differential Equations*, 3(2):253–271, 1995.

[19] P. Mascarenhas. Diffusion generated motion by mean curvature. CAM Report 92-33, UCLA, July 1992. (URL = http://www.math.ucla.edu/applied/cam/index.html).

[20] B. Merriman, J. K. Bence, and S. Osher. Motion of multiple junctions: a level set approach. *Journal of Computational Physics*, 112(2):334–363, 1994.

[21] B. Merriman, J. K. Bence, and S. J. Osher. Diffusion generated motion by mean curvature. In J. Taylor, editor, *Proceedings of the Computational Crystal Growers Workshop*, pages 73–83. AMS, 1992.

[22] W. W. Mullins. Two dimensional motion of idealized grain boundaries. *J. Appl. Phys.*, 27:900–904, 1956.

[23] D. Mumford and J. Shah. Optimal approximations by piecewise smooth functions and associated variational problems. *Communications on Pure and Applied Mathematics*, 42:577–685, 1989.

[24] C. Rottman and M. Wortis. Equilibrium crystal shapes for lattice models with nearest and next-nearest-neighbor interactions. *Physical Review B*, 29(1):328–339, 1984.

[25] S. J. Ruuth. Efficient algorithms for diffusion-generated motion by mean curvature. *Journal of Computational Physics*, 144:603–625, 1998.

[26] S. J. Ruuth and B. Merriman. Convolution generated motion and generalized Huygens' principles for interface motion. *SIAM Journal on Applied Mathematics*, 60:868–890, 2000.

[27] S. J. Ruuth and B. Wetton. A simple scheme for volume-preserving motion by mean curvature. *Journal of Scientific Computing*, 19(1):373–384, 2003.

[28] X. Xu, D. Wang, and X. Wang. An efficient threshold dynamics method for wetting on rough surfaces. *arXiv:1602.04688*, February 2016.